Full Paper

The Redox Behaviour of Randomly Dispersed Single Walled Carbon Nanotubes both in the Absence and in the Presence of Adsorbed Glucose Oxidase

Michael E. G. Lyons [1],* and Gareth P. Keeley [1]

Physical and Materials Electrochemistry Laboratory, School of Chemistry, University of Dublin, Trinity College, Dublin 2, Ireland

* Author to whom correspondence should be addressed; E-mail: melyons@tcd.ie

Abstract: The electrochemical behaviour of SWCNTs randomly dispersed on gold and glassy carbon electrode surfaces was characterised via cyclic voltammetry and complex impedance spectroscopy, using the ferri/ferrocyanide couple as a redox active test probe . In subsequent investigations glucose oxidase (GOx) was adsorbed onto the SWCNT ensemble without apparent denaturation of the enzyme. Cyclic voltammetry and potential step chronoamperometry were used to quantify and understand the process of electron transfer between the immobilised protein redox site and the working electrode. The effect of pH on the system was also investigated. In particular, we have shown that, for the calculation of electron transfer rate constants for surface-immobilised redox systems, chronoamperometry is preferable to voltammetry, which has been the technique of choice until now.

Keywords: Glucose Oxidase; SWCNT-modified electrode; Direct electrochemistry; Chronoamperometry of surface-immobilised systems.

Introduction

Since the discovery of carbon nanotubes (CNTs) by Iijima in 1991 [1], there has been an explosion of research into the physical and chemical properties of these fascinating structures. CNTs can be described as sp^2 carbon atoms arranged in graphitic sheets seamlessly wrapped into cylinders and capped by fullerene-like hemispheres. Single-walled carbon nanotubes (SWCNTs) display excellent chemical stability, good mechanical strength and a range of electrical conductivity. They are at least

ten times stronger than steel, around six times lighter and, depending on their chirality and diameter, can behave as metals, semiconductors or insulators. In a typical sample, around one third can be thought of as metallic. Due to their high surface energies, SWCNTs are usually found in bundles composed of tens to hundreds of tubes in parallel and in contact with each other. Multi-walled carbon nanotubes (MWCNTs) comprise of several layers of graphitic cylinders, which are concentrically nested like the rings of a tree trunk. They are regarded entirely as metallic conductors, which in some respects makes them more suitable for electrochemical applications. However, SWCNTs are more well-defined systems, making their electrochemical properties easier to understand. The electrochemical properties of both multi (MWCNT) and single walled (SWCNT) carbon nanotubes have not been extensively examined to date, although these materials should serve as excellent candidates for nanoelectrodes and platforms for nanoelectrochemical cells and amperometric biosensor devices [2,3].

Electron transfer in biological systems is one of the leading areas in the biochemical and biophysical sciences [4], and in the past few years there has been considerable interest in the direct electron transfer between redox proteins and electrode surfaces. The direct electrochemistry of the heme proteins and flavo enzymes has been widely investigated since the 1970s. Glucose oxidase (GOx) is a large, dimeric protein with a formula weight of 160 kDa. It catalyses the oxidation of β-D-glucose to δ-D-gluconolactone. Glucose oxidase contains one tightly-bound flavin adenine dinucleotide (FAD) unit per monomer. These redox-active prosthetic groups are not covalently bound and may be released from the protein during denaturation. However, in the absence of mediating small molecules, well-defined electrochemical behaviour of flavoprotein-oxidase systems such as GOx is rendered extremely difficult because the flavin adenine dinucleotide (FAD) prosthetic group is embedded deep within the protein structure.

Various immobilization strategies [5,6] have been adopted to fabricate enzyme electrodes for biosensor applications. These strategies have exhibited varying degrees of success and in many cases electron transfer mediators have to be used to facilitate electronic communication between the active site of the protein and the underlying electrode. However the potential at which an amperometric enzyme biosensor is operated depends upon the redox potential of the mediator used rather than that exhibited by the active site of the redox enzyme. Usually the difference in magnitude between the latter potentials is significant (ca. 0.3 - 0.5 V) a factor which acts against successful biosensor operation, since the more positive the operating potential, the greater is the tendency for the sensor to respond to oxidizable substances present in the sample other than the target substrate.

Clearly, the best strategy for successful enzyme biosensor fabrication is to devise a configuration by which electrons can directly transfer from the redox center of the enzyme to the underlying electrode. This has been accomplished in recent years using the idea of molecular wiring. Hence the enzyme can be modified with electron relays, through modification of the peripheral oligiosaccharide with relay species pendant on the termini of flexible spacer chains, and indeed through relays in electron conducting hydrogels within which enzymes are covalently bound.

The similarity in length scales between nanotubes and redox enzymes suggest the presence of interactions that may be favourable for biosensor electrode applications [7]. The strategy of physical adsorption or covalent immobilization of large biomolecules onto the surface of immobilized carbon nanotubes may well represent an exciting pathway through which direct electrical communication

between electrodes and the active site of redox-active enzymes can be achieved. It is hoped that the electrocatalytic properties of carbon nanotubes will have applications in the development of enzyme biosensors without mediators. Indeed recent work reported in the literature suggests that this objective might well be feasible. For instance recent work [8,9] has indicated that the chemical modification of electrode surfaces with carbon nanotubes has enhanced the activity of electrode surfaces with respect to the catalysis of biologically active species such as hydrogen peroxide, dopamine and NADH.. Furthermore, multiwalled carbon nanotubes have exhibited good electronic communication with redox proteins where not only the redox center is close to the protein surface such as in Cytochrome c , azurin and horseradish peroxidase, but also when it is embedded deep within the glycoprotein such as is found with glucose oxidase [10,11]. In many situations the nanotubes are dispersed on the surface of a support electrode to form a randomly dispersed array of high surface area, or else incorporated as a dispersion within a matrix to form a thin film. In a notable paper described recently [12] direct electrical wiring of glucose oxidase to a support electrode has been achieved using well ordered arrays of carbon nanotubes .

In the present paper we focus on two topics. The first is an examination of the electrochemical behaviour of a solution phase redox test couple at an electrode modified with a mesh of SWCNT material randomly dispersed on the surface of the latter, using electrochemical techniques such as cyclic voltammetry and complex impedance analysis. The second aspect of the paper concerns the examination of the redox chemistry of GOx adsorbed on the SWCNT mesh. Standard transient electrochemical techniques such as cyclic voltammetry and potential step chronoamperometry have been used to investigate the process of electron transfer between the immobilised protein redox site and the working electrode. We choose glucose oxidase as a model system precisely because its electrochemical behaviour is well established. Our particular focus in this paper is to establish a procedure by which the most effective quantitative analysis of the electron transfer dynamics between adsorbed biomolecule and electrode surface may be established, and to develop and indeed extend theoretical descriptions by which this quantitative analysis can be made. In particular, we utilise a Gaussian model [13] for investigation of the kinetics of the $FAD/FADH_2$ transition, which we believe is more appropriate than any others applied to analyse the kinetics of surface-immobilised redox enzymes to date.

Experimental

Chemicals

Glucose oxidase (GOx, Type VII, from Aspergillus Niger, 198 U/mg), Nafion (~5% in a mixture of lower aliphatic alcohols and water), potassium ferricyanide and potassium chloride were purchased from Sigma and used as received. Single-walled carbon nanotubes (SWCNTs), HIPCO type, were purchased from Carbon Nanotechnologies Inc., Houston, Texas, USA. Typically the iron content is 15% by mass. All other chemicals were of analytical grade. All solutions were prepared using millipore water. A standard 50 mM pH 7 phosphate buffer was purchased from Sigma and employed as supporting electrolyte except in the pH studies (Section 3.1.2). For these experiments acetate, phosphate and ethanolamine buffers of various pH values were used.

Electrode Modification

A suspension of single-walled carbon nanotubes was prepared by adding SWCNTs (1 mg) to dimethyl formamide (10 cm^3) and sonicating for five minutes. This suspension (1 μL) was cast on inverted gold and glassy carbon macroelectrodes and the DMF was evaporated using a fan heater at 40 °C for approximately fifteen minutes. The electrode was rinsed sequentially with water and working electrolyte before all experiments. A solution of glucose oxidase was prepared by adding GOx (3 mg) to a 50 mM pH 7 phosphate buffer solution (1 cm^3). This solution (10 μL) was deposited on a SWCNT-modified electrode and the solvent was allowed to evaporate at room temperature for approximately 2.5 hours. Finally, Nafion (1 μL) was cast and allowed to dry at room temperature. The resulting film covered the gold and the surrounding epoxy encasement, and was clearly visible to the naked eye. An AFM image recorded for the nanotube dispersion is presented in figure 1. The random dispersed nature of the assemble is apparent from the figure.

Apparatus

A CH Instruments Model 440 potentiostat was used to perform all electrochemical experiments, along with a conventional three-electrode cell. Platinum wire and Ag/AgCl were used as counter and reference electrodes, respectively. Buffers were purged with high-purity nitrogen for at least twenty minutes prior to experiments and a nitrogen environment was then maintained over solutions in the cell throughout all scans. All work was performed at room temperature (20 ± 3 °C).
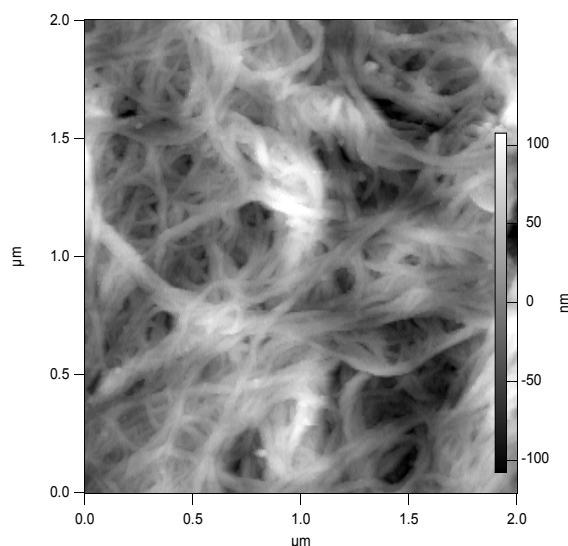
Figure 1. AFM image recorded for ensemble of SWCNT dispersed randomly on a silicon surface.

Results and Discussion

Electrochemical characterization and electron transfer dynamics at SWCNT modified gold and glassy carbon electrodes

Single walled carbon nanotubes may be deposited either as random dispersions or ordered arrays. We expect that the redox response exhibited by carbon nanotube modified electrodes will depend to a large extent on the manner in which the nanotubes are aligned with respect to the support electrode surface. The oxidation of ferrocyanide to ferricyanide in aqueous solution has served as a benchmark reaction in fundamental electrochemistry since the $Fe(CN)_6^{4-/3-}$ reaction involves the transfer of a single electron and exhibits close to ideal quasi-reversible outer sphere kinetic behaviour, especially at electrodes such as carbon where there is minimum bonding (or adsorption) interaction between the electrode material and the reactant (and indeed spectator) ions in solution.

The cyclic voltammetric response profile for a quasi-reversible electron transfer reaction has been the subject of quantitative mathematical analysis, especially in a classic paper by Nicholson [14]. The net shape of the voltammetric curves have been shown to depend on a kinetic parameter ψ which is given by the expression :

$$\Psi = \frac{\left(D_O/D_R\right)^{\alpha/2} k^0}{\left(\pi D_O F \upsilon / RT\right)^{1/2}} \cong \frac{k^0}{\left(\pi D F \upsilon / RT\right)^{1/2}} \tag{1}$$

where we have assumed for simplicity that the diffusion coefficient for the oxidized (O) and reduced (R) forms of the solution phase probe redox couple are equal and that the transfer coefficient α is ½. A numerical analysis of the diffusion boundary value problem for cyclic voltammetry has established a quantitative analysis of the relationship between the kinetic parameter Ψ and the voltammetric peak separation ΔE_p. This is illustrated as a working curve in figure 2 below. For $n\Delta E_p \geq 140$ mV this plot is essentially linear, and Ψ may be calculated by using the following equation:

$$\log \Psi = -5.36 \times 10^{-3} \times n\Delta E_p + 0.15 \tag{2}$$
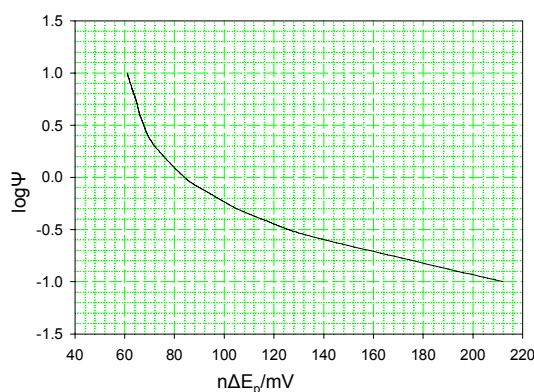
Figure 2. The variation of the kinetic parameter Ψ with voltammetric peak separation .

Hence it is straightforward to determine the standard heterogeneous rate constant k^0 for an interfacial electron transfer reaction, by noting the voltammetric peak separation at a given scan rate v, and using the working curve outlined in figure 1 to determine the corresponding value of the parameter Ψ. The heterogeneous rate constant k^0 may then be determined provided that the diffusion coefficient D of the redox reactant species is known. We note that the smaller the peak separation ΔE_p observed, the larger is the rate constant k^0, and consequently the more facile are the ET kinetics.

It has been established that the cyclic voltammetry response for the $Fe(CN)_6^{4-/3-}$ probe reaction at the basal plane of highly ordered pyrolytic graphite (HOPG) is quasi-reversible with very large peak potential separation ΔE_p typically greater than 700mV (although with surface treatment these values can be reduced to ca. 100 mV), indicative of very sluggish electron transfer kinetics. On graphite edge planes, interfacial Electron transfer occurs much more rapidly with ΔE_p values of 70 mV (recorded at the same sweep rate) being typical.

In our experiments, cyclic voltammetry for ferricyanide reduction was performed using 1 mM ferricyanide reagent in 50 mM KCl / 50mM phosphate buffer solution (pH 7). The scan rates employed (the latter determining the range of experimental timescales) were in the range 5 – 1000 mVs^{-1}.

In figure 3 we outline a comparison between voltammograms obtained using a bare and SWCNT-modified gold working electrodes. Clearly, the SWCNT-modified electrode gives rise to larger ferricyanide reduction peak currents. It is immediately obvious that the peak current for the reduction of ferrocyanide ion is greater for the SWCNT modified electrode than for the unmodified gold electrode. This probably reflects the greater surface area of the nanotube modified electrode. It may also be due to the increased rate of diffusive mass transport of the ferrocyanide reactant to the nanotube surface (the latter being considered as a supported nanoelectrode).
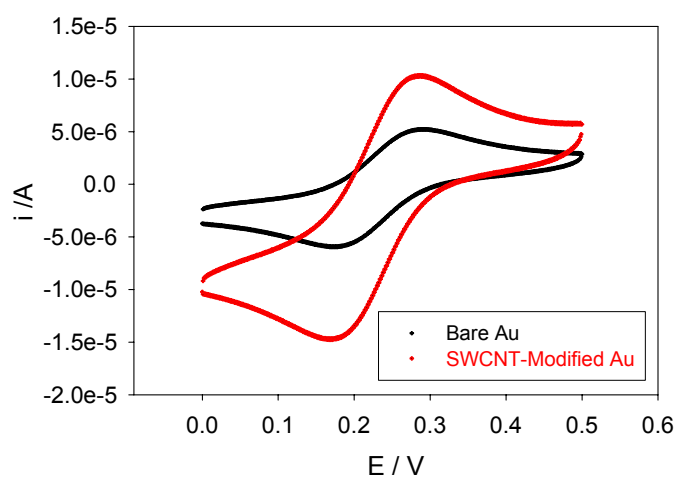
Figure 3. Comparison between voltammograms obtained using a bare and SWCNT-modified gold working electrode. The scan rate employed was 100 mVs^{-1}. The electrolyte used was 1mM potassium ferricyanide in 50 mM KCl in 50 mM phosphate buffer (pH 7).

The peak heights recorded from the cyclic voltammogram for oxidation and reduction should vary in a linear manner with the square root of the scan rate according to the Randles-Sevcik (RS) equation:

$$i_p = 0.4463nFA\sqrt{\frac{nF}{RT}}c^{\infty}\sqrt{D\upsilon} \tag{3}$$

Here, n is the number of electrons lost or gained in the redox process (for this system n = 1), A is the surface area of the electrode in m^2 (for a macroelectrode of radius 1mm, A = 3.14 × 10^{-6} m^2), c^{∞} is the concentration of the electroactive species ($molm^{-3}$) and ν is the sweep rate (Vs^{-1}). Figure 4(a) shows a comparison between Randles-Sevcik plots obtained for the reduction of ferricyanide using a bare and SWCNT-modified Au working electrode. Figure 4(b) shows the corresponding comparison for the oxidation of ferrocyanide. In both cases we note that the Randles-Sevcik slopes for the nanotube modified gold surface are greater than the same parameter recorded for the unmodified electrode. In the case of ferricyanide reduction, the RS slopes were 2.0 × 10^{-5} (r^2 = 0.9991) and 4.5 × 10^{-5} (r^2 = 0.9997) $As^{1/2}V^{-1/2}$ for the bare and SWCNT-modified electrodes respectively. Using the RS equation, the slope of these plots (m_{R-S}) is related to the diffusion coefficient according to: $m_{R-S} = 0.4463nFA\sqrt{\frac{nF}{RT}}c^{\infty}\sqrt{D}$. Since the slope is proportional (for a given bulk concentration of reactant species) both to the surface area of the working electrode and to the diffusion coefficient of the electroactive reactant, it is clear that the larger slope found for the SWCNT-modified electrode was due to increased surface area, since the diffusion coefficient is a parameter characteristic of the solution phase reactant and not the nature of the electrode.

(a)   (b)
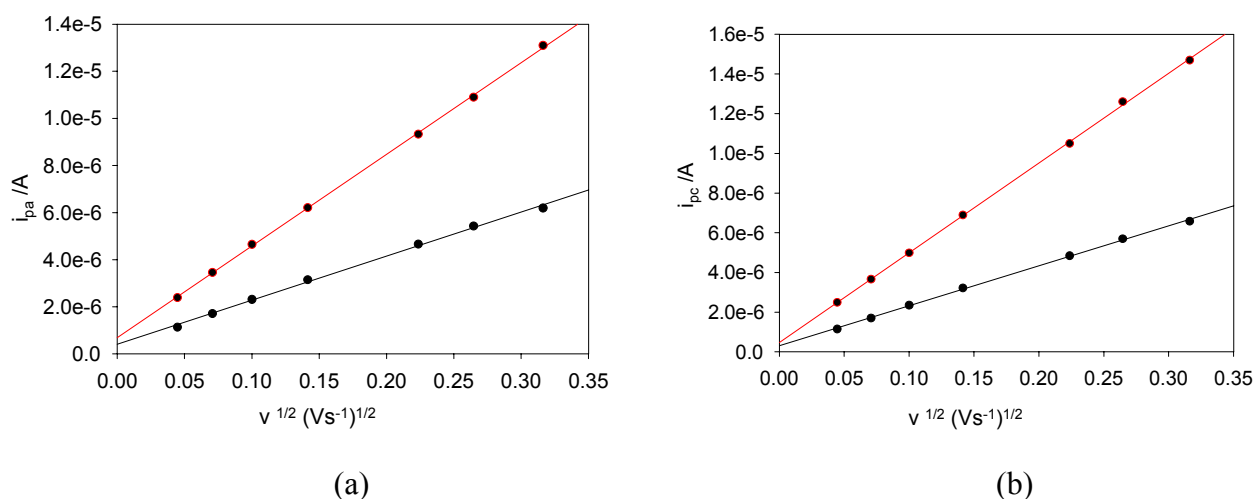
Figure 4. Randles-Sevcik Plots for (a) ferricyanide reduction and (b) ferrocyanide oxidation at bare and SWCNT modified gold electrodes. The upper curve denotes the SWCNT modified electrode data in each case.

The bare Au data were used to calculate the diffusion coefficients for the oxidized $[Fe(CN)_6]^{2-}$ and reduced $[Fe(CN)_6]^{3-}$ species. From the plots, the respective Randles-Sevcik slope values are $m_O = 1.9 \times 10^{-5}$ and $m_R = 2.0 \times 10^{-5}$ $As^{1/2}V^{-1/2}$ respectively. These were used to calculate the corresponding diffusion coefficients $D_O = 5.1 \times 10^{-6}$ and $D_R = 5.6 \times 10^{-6}$ cm^2s^{-1}. The diffusion coefficients for ferrocyanide and ferricyanide are approximately equal. This is to be expected since both complex ions

are approximately the same size , are both octahedral, and do not differ very much in solvated environment. In further experiments we have shown that linear RS behaviour is not observed at higher sweep rates which suggests that the ET reaction becomes quasi-reversible under such conditions.

Further evidence for the decrease in reversibility at higher sweep rates is provided by the variation of the oxidation to reduction peak ratio i_{pa} / i_{pc} with sweep rate ν (see Figure 5). For a perfectly reversible system, this number should always be unity. As can be seen, for both the bare and modified working electrodes, the observed ratio departs steadily from this value as the scan rate increases. Clearly, the ET is not reversible on the smaller timescales (larger sweep rates). For reversible systems, the ET rates at all potentials are significantly greater than the rate of mass transport and therefore Nernstian equilibrium is always maintained at the electrode surface. At low sweep rates, the ET rate may be greater than the rate of mass transport and a reversible scan may be obtained, even if the process is irreversible.
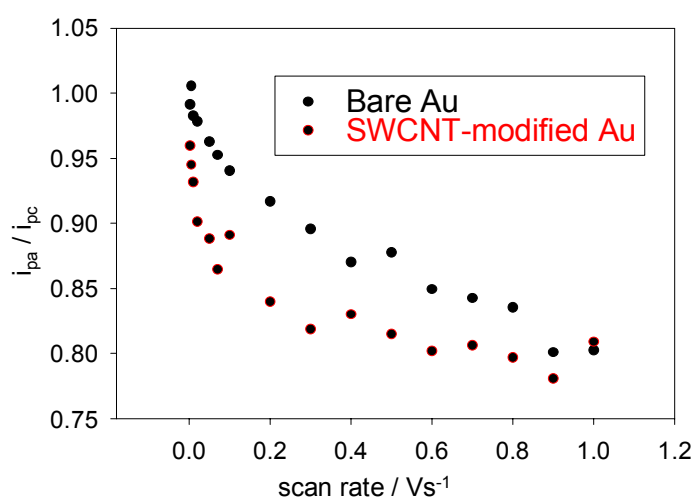
Figure 5. The variation of the ratio of the anodic to the cathodic peak currents with scan rate for a bare and SWCNT-modified Au working electrode. The electrolyte used was a 1mM solution of ferricyanide in 50 mM KCl in a 50 mM PBS (pH 7).

Shown below in figure 6 is a comparison between the variation of peak separation with scan rate for a bare and a SWCNT-modified gold electrode. It is clear from the plot that the SWCNT modified electrode exhibits more facile ET kinetics compared with the unmodified gold surface at higher scan rates since the peak separation values are considerably smaller under these conditions. However, littler difference was observed at lower scan rates. The ΔE_P data over a wide range of sweep rates was analysed using the theory discussed previously in conjunction with the working curve presented in figure 3 .This protocol was used to calculate the Ψ parameter appropriate for a given peak separation value and scan rate and hence to evaluate heterogeneous ET rate constants for each scan rate used. The average k^0 values were found to be $(6.2 \pm 1.4) \times 10^{-3}$ and $(10.2 \pm 5.1) \times 10^{-3}$ cms^{-1} for the bare and SWCNT-modified Au electrodes respectively. We note that our SWCNT modified gold electrodes are not as catalytically active as those reported recently by Nugent and co-workers [15]. The latter reported similar experiments conducted on MWCNT modified platinum electrode surfaces and reported that the ET rate constant for ferrocyanide oxidation is $k^0 \approx 0.5$ cm s^{-1} .

Similar experiments were carried out using SWCNT dispersed on glassy carbon support electrodes. Here, the rate constants were found to be $(2.7 \pm 0.6) \times 10^{-3}$ and $(4.2 \pm 0.1) \times 10^{-3}$ cms^{-1} for the bare and SWCNT-modified GC electrodes, respectively. It is interesting to note that the presence of the nanotubes enhances the rate constant by the same factor, 1.6, for both gold and glassy carbon. This finding indicates that dispersions of SWCNTs display well-defined and reproducible electrochemistry, despite their random arrangement. The better performance of the SWCNT electrodes has been attributed to the NT dimensions, structure, and to topological defects present on the tube surface [16].
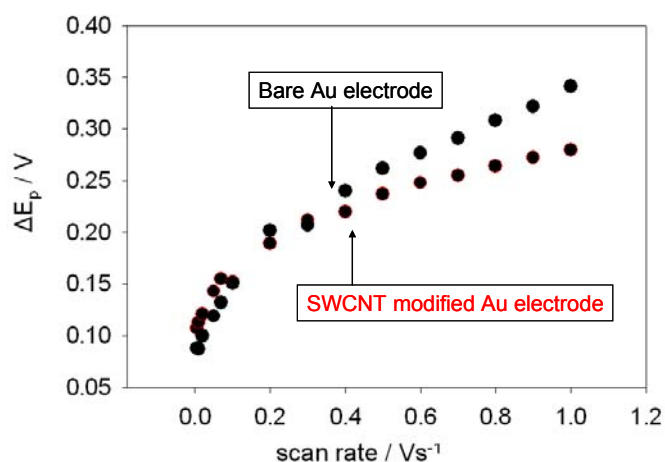
Figure 6. The variation of peak separation with scan rate. The electrolyte used was a 1mM solution of ferricyanide in 50 mM KCl in a 50 mM Phosphate buffer solution (pH 7).

The rate constant for heterogeneous ET between a solution phase redox couple and an electrode can be calculated using a number of different approaches. The theories of ET reactions can be classified into two groups. The first are the classical or semi-classical theories derived from the models of Hush and Marcus. These are based on the transition state theory or its modern extensions, and pertain to the adiabatic limit in which the interaction between the electrode and the reactant is strong. The second group are quantum theories based on the work of Levich and Dogonadze which rely on perturbation theory and presume a weak interaction between the electrode and the reactant and so deal with non-adiabatic ET. Both classes of theories have been reviewed recently [4]. In short the heterogeneous rate constant depends on the product of the density of electronic states in the metal and the transition probability for ET across the interface integrated over all available energies. It is expected that the local density of electronic states of a SWCNT will differ significantly from that of a bare metal. This may well explain the difference in rate constants observed.

Furthermore it has been suggested [17] that the immobilized SWCNT species act as electron transfer relay stations and mediate electron exchange between the underlying metal electrode and the redox couple in solution. The density of electronic states distribution diagram for a SWCNT modified gold electrode in contact with an electrolyte solution containing a redox active couple such as ferricyanide is outlined in figure 7. The filled electronic states are shaded and the situation at equilibrium (fig.7(a)) and under cathodic polarization (fig.7(b)) are illustrated. At equilibrium the

Fermi levels of Au, SWCNT and redox couple are all located at the same position. When the potential is swept in the negative direction away from the equilibrium value the Fermi level $E_{F,Au}$ is raised and exceeds $E_{F,SWCNT}$. Consequently electrons are injected into the unoccupied energy states of the SWCNT via through space electron tunneling to make $E_{F,SWCNT} = E_{F,Au}$. The increased value for the Fermi energy of the SWCNT species results in a significant overlap between the Gaussian density of states curve for the oxidized form of the redox couple (i.e. ferricyanide) and that of the filled SWCNT levels. Hence the transition probability of electron transfer from the SWCNT to the oxidized form of the redox couple is greatly enhanced . Conversely the degree of overlap between SWCNT filled levels and the Gaussian density of states curve for the reduced form of the redox couple (i.e. ferrocyanide) is significantly reduced and oxidation is disfavoured. Hence an enhanced reduction current is observed. Conversely if the potential is scanned in a direction positive from that corresponding to the equilibrium value the $E_{F,Au}$ value is decreased, which causes a corresponding fall in the value of $E_{F,SWCNT}$. When the potential is such that $E_{F,Au}$ is less than the equilibrium value, the value of $E_{F,SWCNT}$ will overlap significantly with the Gaussian maximum density of states of the reduced form of the redox couple and the probability of electron transfer from the reduced species energy levels to the SWCNT will be enhanced and a net oxidation current occurs. Hence this simple energy level picture can explain the voltammetric results illustrated in figure 3.
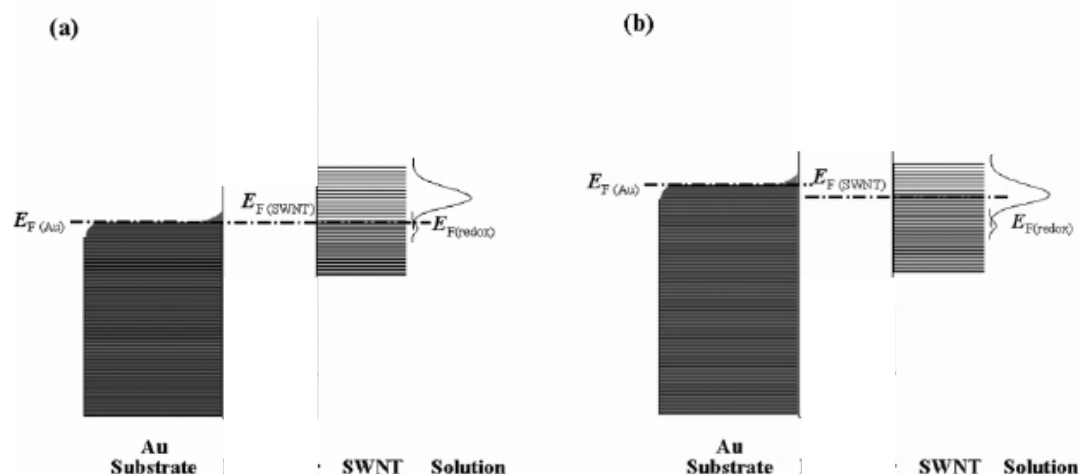
Figure 7. The variation of peak separation with scan rate. The electrolyte used was a 1mM solution of ferricyanide in 50 mM KCl in a 50 mM Phosphate buffer solution (pH 7) (adapted from ref.17).

It is reasonable to suppose that the large pi-conjugated system within the SWCNT 'molecule' confers properties both of electron acceptor and electron donor to the latter. Under cathodic polarization the adsorbed SWCNT accept electrons from the gold thereby increasing the filled energy levels in the SWCNT, thereby enabling electrons to be donated to acceptor redox couples in solution.

Correspondingly during anodic polarization SWCNT molecules donate electrons to the gold electrode and simultaneously accept electrons from donor redox couples in solution. The large number of occupied and unoccupied energy states within the SWCNT allows not only facile ET between the adsorbed SWCNT and the redox couple in solution but also efficient electron tunneling between the SWCNT and the electrode substrate.

Hence when considering the redox behaviour of SWCNT modified electrodes in contact with solution phase redox couples, three distinct kinetic processes must be considered: (i) electron tunneling from gold/glassy carbon surface to SWCNT ; (2) electron transport within SWCNT and (3) heterogeneous ET from SWCNT ends or sidewalls to $Fe(CN)_6^{3-}$ molecules in solution. If it assumed that electron transport through the nanotube is rapid then the observed redox response may be attributed either to electron tunneling from the support electrode surface to the adsorbed nanotube, or to slow electron transfer kinetics of the solution phase redox couple at the sidewalls and ends of the nanotubes. The situation may be represented in terms of a simple electrical equivalent circuit as illustrated in figure 8.
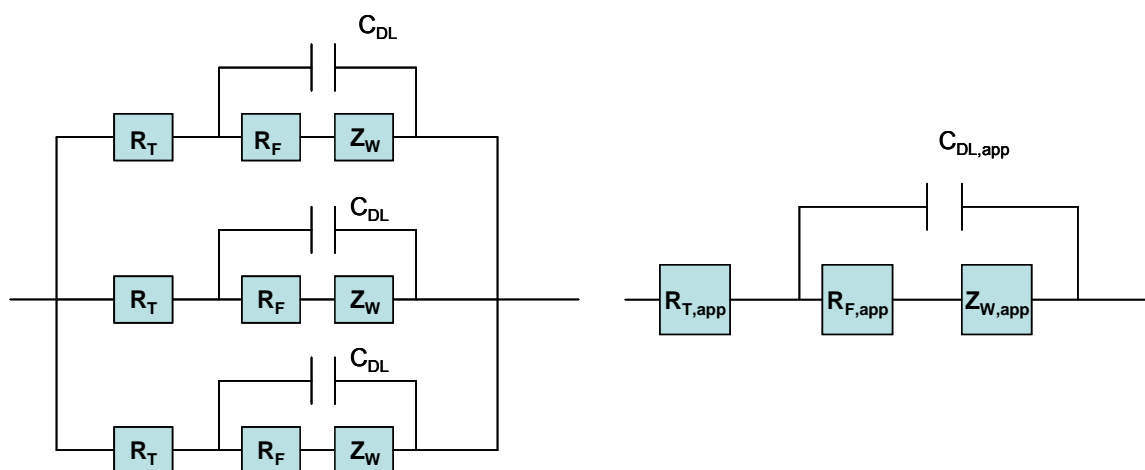
Figure 8. Electrical equivalent circuit of ensemble of randomly dispersed SWCNT on metal support surface.

In this figure we represent the redox behaviour of the immobilized nanotubes in terms of an electrical equivalent circuit [17] consisting of a number of parallel branches each consisting of a tunneling resistance R_T in series with another circuit element consisting of a parallel combination of a double layer capacitor C_{DL} in, a Faradaic charge transfer resistance R_F and a Warburg diffusion impedance Z_W. This equivalent circuit represents an ensemble of SWCNT's immobilized randomly on the surface of a gold support electrode. We expect that a certain degree of dispersion with respect to energy and kinetic activity will be exhibited by the immobilized ensemble. If no such energy dispersion exits then one can predict that the equivalent circuit illustrated on the right hand side of figure 8 reduces to the simple set of circuit elements presented on the left hand side of figure 8 , where the energy distributed elements are replaced by 'apparent' or energy averaged quantities. We can readily show that the impedance response of this type of circuit configuration in the complex plane [18] consisting of an Nyquist plot of Imaginary part Im(Z) = Z'' of the total impedance versus real part

of the impedance Re(Z) = Z',   is a depressed semicircle at high frequencies followed by a linear feature at lower frequency. The high frequency semicircle represents the heterogeneous ET kinetics between the nanotube and the solution phase redox reactant, whereas the low frequency linear feature is associated with the diffusive transport of the solution phase redox couple to the nanotube surface. Furthermore the real axis intercept at high frequency is associated with the sum of tunneling and solution resistance.

We have performed a series of preliminary experiments to measure the complex impedance response of SWCNT randomly dispersed and immobilized both on gold and glassy carbon electrodes in contact with aqueous solutions containing the ferrocyanide/ferricyanide redox couple, and compared these results with analogous data obtained for the respective unmodified electrodes. We determined the impedance response of both unmodified and SWCNT modified gold electrodes over a wide range of frequencies, typically from an upper limit of 100 kHz to a lower limit of 1 Hz. Typical Nyquist data obtained from such experiments are presented in figure 9 and 10 below. Each data point corresponds to a discrete frequency measurement. The measurements were obtained when the electrode was polarized at a dc potential of 0.23 V corresponding to that of the standard potential of the $Fe(CN)_6^{3-/4-}$ redox couple. We note from figure 9 that depressed semi-circle features are observed at high frequencies and well defined linear Warbourg diffusive features are present at lower frequencies both for the unmodified gold electrode and the SWCNT modified gold electrode. This is in accordance with the basic equivalent circuit description presented in figure 8. Furthermore the amplitude of the high frequency semicircle is much smaller for the SWCNT modified electrode indicating the occurrence of faster heterogeneous electron transfer kinetics and electron injection via tunneling at the latter modified electrode compared with the unmodified electrode.
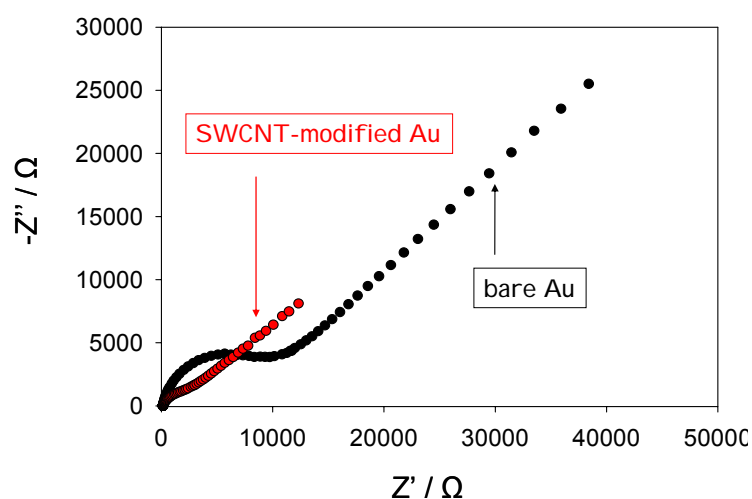
Figure 9. Complex impedance Nyquist plots recorded for ferricyanide reduction at Au and SWCNT modified Au electrodes.

A similar set of impedance experiments were conducted on unmodified glassy carbon and SWCNT-modified glassy carbon electrodes. The results of these experiments are presented in figure 10 below.

Again both a depressed semicircle observed at high frequencies followed by a Warbourg feature at lower frequencies may be noted both for the unmodified and SWCNT modified GC electrodes. In contrast to that seen with gold the high frequency semicircle is larger when the GC electrode is modified with the dispersed nanotube assembly.

General electrochemical properties of SWCNT/GOx-modified electrodes

   In this section of the paper we concentrate on examining the general electrochemical characteristics of glucose oxidase which has been adsorbed on an assembly of single walled carbon nanotubes randomly dispersed both on gold and glassy carbon support electrode surfaces. A typical AFM image recorded for a nanotube assembly (dispersed in this case on a silicon surface) on which glucose oxidase has been adsorbed is outlined in figure 11. It is clear from the latter image that the enzyme fills much of the void space between the nanotube fibres. Hence we expect that the enzyme loading should be at a level to ensure good catalytic activity. In our experiments the gold electrodes were initially modified with an assembly of SWCNT as outlined previously. The SWCNT modified Au (or glassy carbon) electrode was then thoroughly washed with water and immersed in a 16 mg mL^{-1} GOx in phosphate buffer solution (0.05 M, KH$_2$PO$_4$ + Na$_2$HPO$_4$, pH 7) at 20^{0}C for ca. 2.5 hours. Adsorption of glucose oxidase onto the SWCNT occurs within this timescale. In some experiments the enzyme SWCNT composite electrode was further modified by depositing a thin layer of soluble nafion via drop coating. The resulting enzyme modified electrodes were then subjected to electrochemical analysis (largely cyclic voltammetry and potential step chronoamperometry) in phosphate buffer solution.
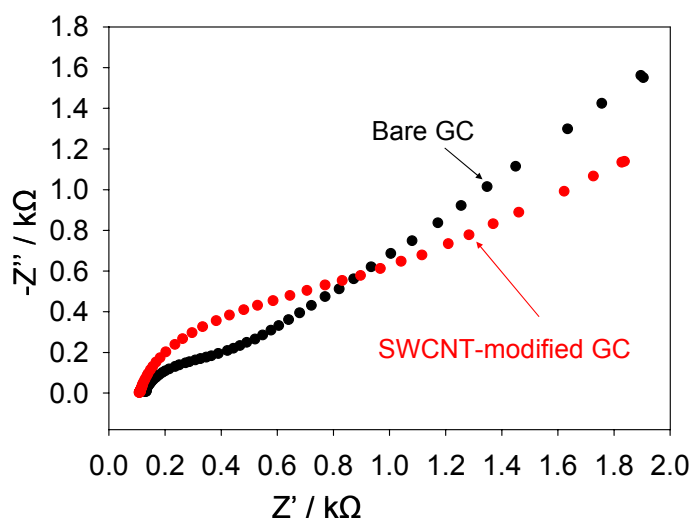
Figure 10. Complex impedance Nyquist plots recorded for ferricyanide reduction at GC and SWCNT modified GC electrodes.

   The electrochemical response of the latter enzyme modified SWCNT modified electrode was determined using cyclic voltammetry. The voltammograms presented in Figure 12 were obtained using a bare, SWCNT-modified and SWCNT/GOx and SWCNT/GOx/Nafion-modified gold working electrodes in a 50 mM phosphate buffer (pH 7). As can be seen, while a bare gold electrode exhibits a

virtually flat and featureless voltammetric response, a pair of well-defined redox peaks was observed at the both the SWCNT/GOX and SWCNT/GOx/Nafion-modified electrode. The observed peaks are characteristic of those representing the redox behaviour of an adsorbed species, in this case that of the flavin adenine dinucleotide FAD. The peaks are reasonably symmetrical and exhibit the characteristic bell shape expected for adsorbed redox species [19]. The absence of any peaks on the SWCNT-modified Au voltammogram suggests that the voltammetric response observed with the latter is essentially capacitive in the absence of any redox active substrates present in the electrolyte solution. It also indicates that the nanotubes are reasonably free from any oxidized functionalities.
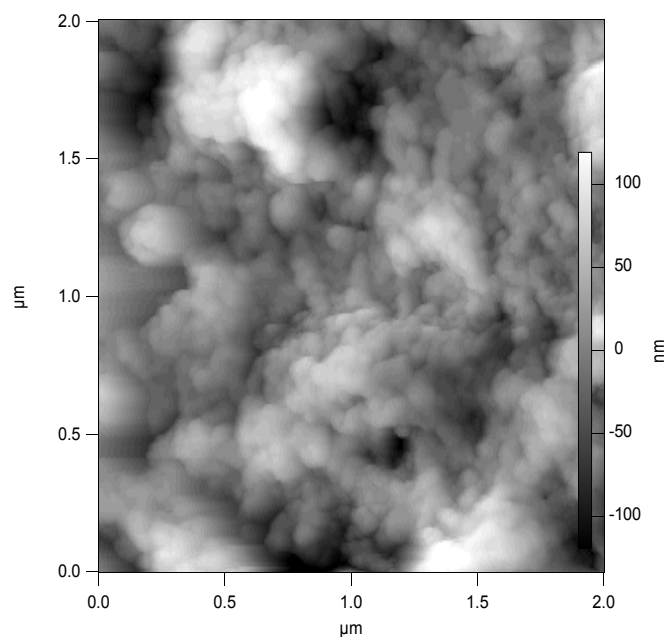
Figure 11. AFM image recorded for a SWCNT assembly dispersed randomly on a silicon surface on which glucose oxidase was adsorbed for a 2.5 hr period at room temperature.

It is interesting to note that the FAD/FADH$_2$ redox peaks are more defined when Nafion is used as an overcoating agent. Without application of the latter the voltammograms are characterized by an ill resolved set of redox peaks superimposed on a rather large capacitive current backgrouns. For the voltammetric response of the SWCNT/GOx/Nafion composite electrode at a sweep rate of 100 mVs^{-1}, the cathodic peak potential (E_{pc}) is -417 mV vs. Ag/AgCl and the peak separation (ΔE_p) is 41 mV. The surface coverage of adsorbed redox enzyme can be calculated by integrating the charge Q under the voltammetric peak using the formula : $\Gamma = Q/nFA$ where A denotes the geometric electrode area , n denotes the number of electrons transferred in the redox process (2 in the present case) and F is the Faraday constant. We estimate that $\Gamma = 1.7$ nmol cm^{-2} for the Nafion coated SWCNT/GOx composite electrode. The corresponding data set for the SWCNT/GOx composite without the Nafion overlayer is a cathodic peak potential (E_{pc})of -449 mV vs. Ag/AgCl and a peak separation (ΔE_p) of 24 mV. It is difficult to estimate the surface coverage for the latter system since the resolution between Faradaic

and capacitive processes is poor. Consequently we do not provide a numerical estimate for this quantity but merely note that it is certainly less that that recorded for the Nafion coated system.
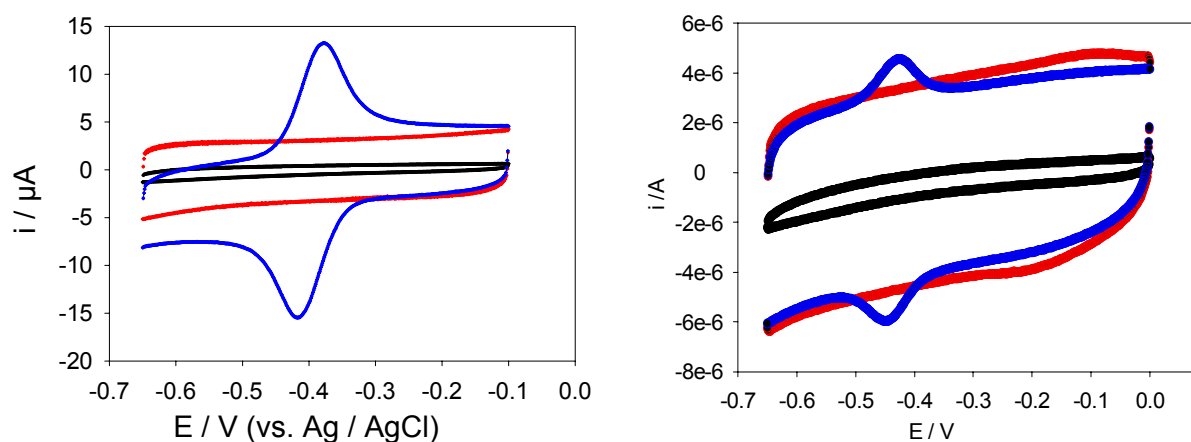
Figure 12. LHS Picture: Cyclic voltammograms recorded at a bare (black), SWCNT-modified (red) and SWCNT/GOx -modified (blue) gold working electrode. RHS Picture: Cyclic voltammograms recorded at a bare (black), SWCNT-modified (red) and SWCNT/GOx/Nafion -modified (blue) gold working electrode The electrolyte used in both sets of experiments was a 50 mM phosphate buffer (pH 7) and the scan rate employed was 100 mVs-1.

In a recent communication Wang and co-workers [20] have reported that SWCNT are readily soluabilised in Nafion solutions made from ethanol or aqueous phosphate buffer. TEM images clearly indicate individual SWCNT ropes when disersed in the latter media. This is in contrast to the high density intertwined aggregates found when SWCNT are dispersed in organic solvents such as chloroform. The structure of Nafion in solution may be viewed as a fluorocarbon backbone with protruding polar sulfonate SO_3^- groups . Hence it is similar in nature to other polymers which have been used to wrap and solubilise CNT material. According to Smalley and co-workers [21] the wrapping of nanotubes by water soluble polymers such as Nafion is a general phenomenon driven by a thermodynamic impetus to eliminate the hydrophobic interface between the tubes and the aqueous medium, thereby reducing the density of the tangled and rather dense tube assembly on the electrode surface. This may well increase the permeability of the void space between the tubes to increased quantities of electrolyte ions which will result in a change in the interfacial potential distribution and hence on the voltammetric response [22].

Ideally ΔE_p should be zero for surface immobilized redox systems, [19,23] . The non zero ΔE_p value observed in both cases above may be attributed to the presence of a potential difference between the electrode and the site of electron transfer (the flavin redox group) [24]. Such a difference would be attributed to the surrounding protein sheath acting as a dielectric layer. The presence of Nafion, while enhancing the discrimination between current resulting the surface redox reacting and the capacitive background contribution, may well result in a larger potential drop in the interface region. The prominent background current is a consequence of the large, catalytically active surface area of the modified electrode [25,26].

The influence of scan rate on the system was investigated within the range of 0.005 to 5.0 Vs^{-1} for gold and 0.002 to 13.0 Vs^{-1} for glassy carbon. Figure 12 shows a comparison between voltammograms obtained at five different scan rates.
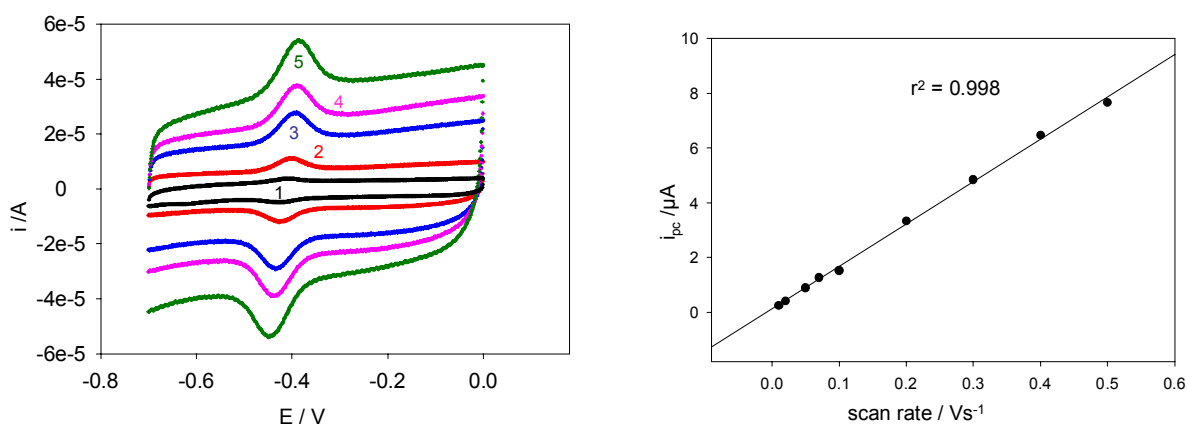
Figure13. (a) Cyclic voltammograms obtained using a SWCNT/GOx-modified Au working electrode. The electrolyte used was a 50 mM PBS (pH 7). The scan rates shown are (1) 0.1, (2) 0.3, (3) 0.8, (4) 1.1 and (5) 1.5 Vs^{-1}. (b) The variation of cathodic peak current with scan rate using a SWCNT/GOx-modified Au working electrode. The electrolyte used was a 50 mM PBS (pH 7).

It was found that the peak currents exhibited a linear relationship with the sweep rate, a feature which is characteristic of surface-bound redox processes as outlined in the analytic theory proposed by Laviron [19,23]. Figure 13(b) shows the variation of i_{pc} with v for lower scan rates. The linearity was reasonably evident over the entire range of sweep rates studied.

The Effect of solution pH on the surface redox behaviour of the FAD/FADH$_2$ couple.

The FAD system involves the transfer of two electrons and an associated protonation/deprotonation equilibrium as illustrated below in scheme 1.

In summary the redox stoichiometry should be described by:

$$FADH_2 \underset{\xrightarrow{}}{\overset{-2e^- -2H^+}{\longrightarrow}} FAD^+$$
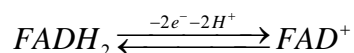
This implies that the redox behaviour exhibited by the flavin groups should depend on the pH of the environment. In figure 14 we present a number of voltammograms recorded in various buffer solutions of known pH. The solution pH values were as follows: 5.2 (acetate buffer), 5.9, 7.0, 8.0 (phosphate) and 8.9 (ethanolamine). As can be seen, the position of the peak potential of FAD depends on solution pH. All changes in voltammetric peak potentials and currents with pH were reversible, that is, the same voltammogram can be obtained if the electrode is transferred from a solution with a different pH value back to its original solution.
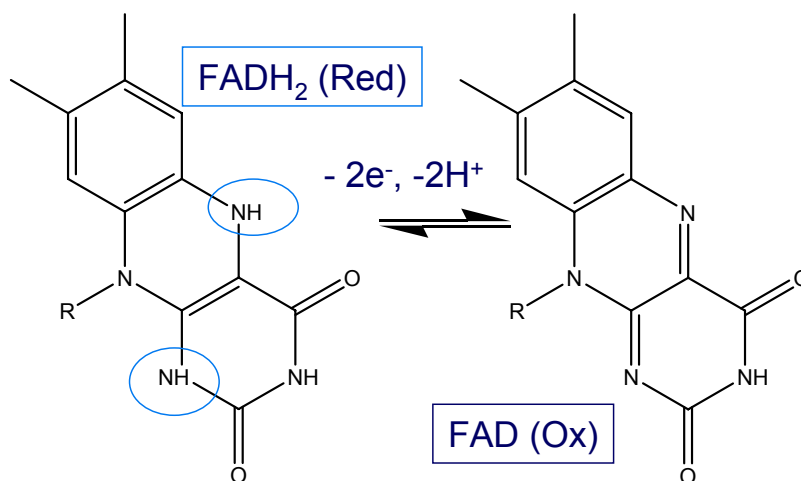
Scheme 1.
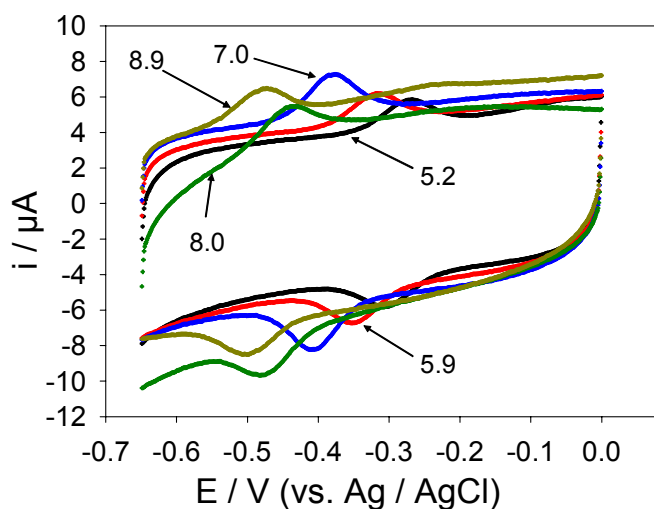
Figure 14. Voltammogams obtained using a SWCNT/GOx/Nafion-modified gold working electrode in buffers of various pH values. The scan rate employed in each case was 100 mVs^{-1}.

Within the pH range studied, the reduction peak potential was observed to shift cathodically with increasing pH value, with a slope of 56 mV per decade change of H$^+$ ion concentration , as shown in Figure 15. This result is in good agreement with the theoretical value of 59 mV per decade change of [H$^+$] for a reversible, two-proton/ two-electron process at 22 °C [16], calculated using the Nernst equation, and also with previous data published by Liang and Zhuobin [27] for adsorbed glucose oxidase on a SWCNT-modified gold electrode (48 mV/decade). Hence the pH studies confirm the stoichiometry of the FAD/FADH$_2$ surface redox reaction as presented in scheme 1 .
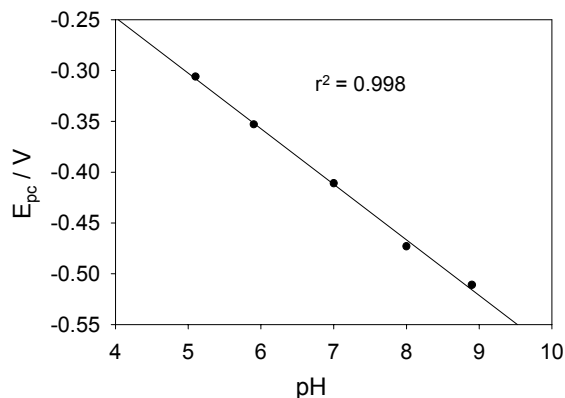
Figure 15. The variation of the cathodic peak potential with pH obtained using a SWCNT/GOx/Nafion-modified gold working electrode in buffers of various pH values. The sweep rate employed in each case was 100 mVs^{-1}.

Having established the details of the thermodynamics and stoichiometry of the adsorbed flavin group we now proceed to use electrochemical techniques to probe and extract quantitative information on the kinetics of the redox transition of the immobilized enzyme molecules. This analysis was accomplished using two techniques, linear potential sweep voltammetry and potential step chronoamperometry. We will contend that the latter method provides a more facile method of data analysis than the former, even though linear potential sweep voltammetry seems to be the method primarily adapted by workers in the field.

Determination of flavin group redox kinetics via lps voltammetry: application of the Laviron Method

Linear potential sweep voltammetry may be used to extract kinetic parameters such as heterogeneous rate constants and transfer coefficients for surface immobilized redox reactions by examining the variation of voltammetric redox peak potential with experimental time scale (i.e. sweep rate). Quantitative data analysis relies on a theoretical methodology originally developed by Laviron [19]. We will briefly summarise this analysis here.

The degree of kinetic reversibility exhibited by a surface redox reaction depends on the experimental timescale. It is expected that a surface redox reaction will exhibit reversible behaviour (manifested as a sweep rate invariant peak potential) when the sweep rate is small, and irreversible behaviour (indicated by a linear variation of peak potential with natural logarithm of sweep rate) when the sweep rate is large. This general expectation was confirmed in our experiments. When the scan rate is higher than 0.2 Vs^{-1}, it was observed that E_{pc} shifts negatively and E_{pa} shifts positively with increasing sweep rate. Figure 15 shows plots of anodic and cathodic peak potential as a function of the natural logarithm of the applied scan rate for a SWCNT/GOx/Nafion-modified gold working electrode. It is clear that the peak potentials are practically invariant with sweep rate when the latter is low, and in contrast for high sweep rates, peak potentials are proportional to ln v.
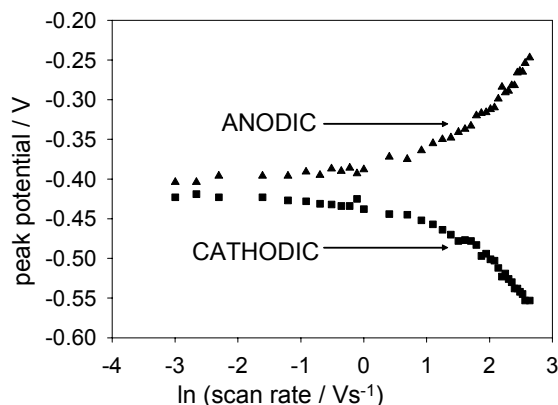
Figure 16. Plots of anodic and cathodic peak potentials against the natural logarithm of scan rate for a SWCNT/GOx/Nafion-modified gold working electrode. The electrolyte used was a 50 mM phosphate buffer (pH 7).

For a surface-bound redox reaction involving redox active enzyme molecules adsorbed on surface immobilized SWCNT meshes, we can show that the following expression holds for the normalized current response for an oxidative potential sweep:

$$\Psi = \frac{i}{nF^2 A\Gamma_\Sigma \upsilon / RT} = m\left\{\left(\eta^\beta + \eta^{-(1-\beta)}\right)X_R - \eta^{-(1-\beta)}\right\} \qquad (4)$$

where i denotes the current, Γ_Σ is the total redox group surface coverage (mol cm^{-2}), υ is the voltammetric sweep rate (V/s), A denotes the electrode area (cm^2) and m is a dimensionless parameter which relates the heterogeneous electron transfer rate constant to the experimental time scale and is given by $m = k_{ET}^0 / \sigma = k_{ET}^0 RT / F\upsilon$. Also in eqn.4 β represents the symmetry factor (typically ½) and $\eta = \exp[\xi]$, where the normalized potential is given by: $\xi = F(E - E^0)/RT$. Finally the mole fraction X_R of reduced enzyme sites adsorbed on the SWCNT mesh is given by the solution to the following differential equation:

$$\frac{dX_R}{d\eta} + \frac{m}{\eta}\left(\eta^\beta + \eta^{-(1-\beta)}\right)X_R = \frac{m}{\eta}\eta^{-(1-\beta)} \qquad (5)$$

This equation may be readily solved for suitable limiting values of the Laviron reversibility parameter m. First when the redox reaction is totally irreversible when $m \to 0$. Under these circumstances $\eta \gg 1, \eta^{-1} \ll 1$ and eqn.5 reduces to:

$$\frac{dX_R}{d\eta} + m\eta^{-(1-\beta)}X_R = 0 \qquad (6)$$

which can be readily integrated to yield

$$X_R \cong \exp\left[-\frac{m}{\beta}\eta^\beta\right] \qquad (7)$$

and also for totally irreversible conditions we have $\eta^\beta \gg \eta^{-(1-\beta)}$ and so the expression for the normalized current response presented in eqn.4 reduces to

$$\Psi \cong m\eta^\beta X_R = m\eta^\beta \exp\left[-\frac{m}{\beta}\eta^\beta\right] \qquad (8)$$

This function exhibits a maximum or peak value designates as Ψ_p when $d\Psi/d\eta = 0$. We can readily show that under such conditions $\eta = \eta_p$ which is a maximum value, and

$$\frac{d\Psi}{d\eta} = \beta m \eta_p^{\beta-1} \exp\left[-\frac{m}{\beta}\eta_p^{\beta}\right] - m^2 \eta_p^{\beta} \eta_p^{\beta-1} \exp\left[-\frac{m}{\beta}\eta_p^{\beta}\right] = 0 \qquad (9)$$

Hence simplifying we obtain

$$\beta - m\eta_p^{\beta} = 0 \qquad (10)$$

which simplifies to

$$\eta_p = \left(\frac{\beta}{m}\right)^{1/\beta} \qquad (11)$$

Substituting eqn.11 into eqn. 8 we end up with the following simple result

$$\Psi_p = \frac{\beta}{e} \qquad (12)$$

In terms of currents we obtain

$$i_p = \frac{\beta}{e}\left\{\frac{nF^2 A\Gamma_\Sigma}{RT}\right\}\upsilon = S_{irrev}\upsilon \qquad (13)$$

We also note that the normalized peak potential function is given by

$$\xi_{p,ox} = \ln\eta_{p,ox} = \frac{1}{\beta}\ln\left(\frac{\beta}{m}\right) = \frac{1}{\beta}\ln\beta + \frac{1}{\beta}\ln\frac{1}{m} \qquad (14)$$

where we have written $\xi_p = \frac{F}{RT}(E_p - E^0) = \theta_p - \theta^0$ and we note that $\theta_p = \frac{FE_p}{RT}$, $\theta^0 = \frac{FE^0}{RT}$ represent normalized potentials. Hence we end up with a useful diagnostic expression for an irreversible surface oxidation reaction

$$\theta_{p,ox} = \theta^0 + \frac{1}{\beta}\ln\beta + \frac{1}{\beta}\ln\frac{1}{m} \qquad (15)$$

where a plot of peak potential versus the natural logarithm of the inverse sweep rate parameter is linear.

It is possible to derive similar expressions for a reductive surface process and we can show that in such a situation:

$$\mathrm{X}_O = \exp\left[\frac{m}{(1-\beta)}\eta^{-(1-\beta)}\right]$$

$$\Psi = m\eta^{-(1-\beta)}\exp\left[\frac{m}{(1-\beta)}\eta^{-(1-\beta)}\right] \qquad (16)$$

and the corresponding peak currents and potentials are given by

$$\Psi_p = -\frac{(1-\beta)}{e}$$

$$\xi_{p,red} = \theta_{p,red} - \theta^0 = -\frac{1}{1-\beta}\ln(1-\beta) - \frac{1}{(1-\beta)}\ln\frac{1}{m} \qquad (17)$$

Furthermore we define $\Delta\theta_p = \theta_{p,ox} - \theta_{p,red}$ as the normalized peak potential difference. This parameter can be used to derive useful kinetic information. We can show that

$$\Delta\theta_p = \frac{1}{\beta(1-\beta)}\ln\frac{1}{m} + \ln\left\{\frac{\beta^{1/\beta}}{(1-\beta)^{1/1-\beta}}\right\} \tag{18}$$

Specifically when the transfer coefficient β = 0.5, eqn.18 becomes $\Delta\theta_p = 4\ln m^{-1}$. This expression will be valid with less than 2% error for $m^{-1} > 12$ which occurs for $\Delta E_P > 200$ mV. We can simplify eqn.18 to obtain the following expression from which the standard rate constant k_{ET}^0 can be derived provided that the transfer coefficient β can be evaluated:

$$k_{ET}^0 = \exp\left[F(\beta) - \frac{\beta(1-\beta)F}{RT}\Delta E_p + \ln\left(\frac{F\upsilon}{RT}\right)\right] \tag{19}$$

where

$$F(\beta) = \beta(1-\beta)\ln\left\{\frac{\beta^{1/\beta}}{(1-\beta)^{1/(1-\beta)}}\right\} = \ln\left\{\frac{\beta^{1-\beta}}{(1-\beta)^{\beta}}\right\} \tag{20}$$

Furthermore from eqn.15 and eqn.17 we note that the normalized peak potential ξ_p will vary in a linear manner with the natural logarithm of the inverse scan rate parameter m^{-1}. Now if the linear portion of the $\xi_{p,ox}$ versus m^{-1} curve is extrapolated to the point where $\xi_{p,ox} = \theta_{p,ox} - \theta^0 = 0$, then at this specific value of the parameter m which we designate as $m_{ox}*$ we note that $\ln\beta + \ln\frac{1}{m_{ox}*} = 0$ or $m_{ox}* = \beta$. This translates to $k_{ET}^0 = \frac{\beta F}{RT}v_{ox}*$. Similarly we can show that $k_{ET}^0 = \frac{(1-\beta)F}{RT}v_{red}*$. Now we can readily evaluate an expression for the transfer coefficient β by noting that

$$\beta = \frac{1}{1 + \frac{v_{ox}^*}{v_{red}^*}} \tag{21}$$

We conclude therefore that from eqn.21 and eqn.19 the fundamental kinetic parameters for an irreversible surface process may be determined via measurement of peak potential and peak potential difference as a function of sweep rate.

Transforming eqn.18 we obtain [19]:

$$\Delta E_p = \frac{RT}{(1-\beta)\beta F}[\beta\ln(1-\beta) + (1-\beta)\ln\beta - \ln\frac{RT}{F} - \ln k_{ET}^0] + \frac{RT}{(1-\beta)\beta F}\ln\upsilon. \tag{22}$$

Peak separations were plotted against lnv for high scan rates (at which the redox process exhibits quasi-reversible/totally irreversible behaviour). Figure 17 shows such a plot for a SWCNT/GOx/Nafion-modified gold electrode. The slope of this graph was found to be 208 mV, with a y-intercept of -234 mV. For the glassy carbon working electrode these values were 122 and -42 mV, respectively. From the slopes, α values of 0.11 and 0.10 were calculated for gold and glassy carbon respectively. These values were used along with the intercepts to calculate a rate constant of 19 s^{-1} for the FAD/FADH$_2$ transformation on gold and 18 s^{-1} for the same process on glassy carbon.
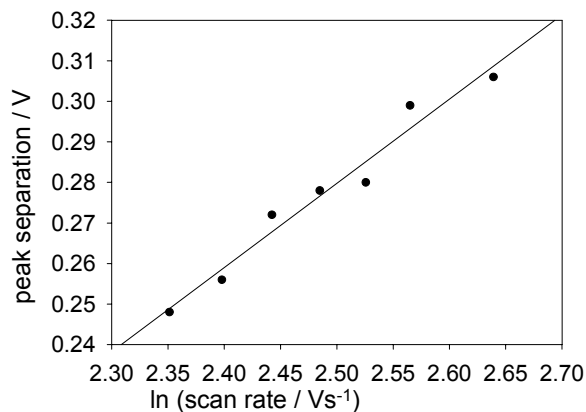
Figure 17. Peak separation against the natural logarithm of scan rate for a SWCNT/GOx/Nafion-modified gold working electrode. The electrolyte used was a 50 mM phosphate buffer (pH 7).

These results may be compared with data previously reported in the literature [27,28]. In this work the apparent heterogeneous electron transfer rate constants for redox proteins and enzymes such as hemoglobin (Hb), horseradish peroxidase (HRP) and Glucose Oxidase (GOx) were determined using linear potential sweep voltammetry at SWCNT modified glassy carbon electrodes to be in the range 1-2 s^{-1}. In contrast Dong and co-workers [29] have examined the kinetics of the microperoxidase 11 redox transformation at glassy carbon electrodes modified with MWCNT meshes. For a microperoxidase loading of 0.84 nmol cm^{-2} a standard rate constant of 38 s^{-1} was determined. It is clear that the standard heterogeneous rate constant for adsorbed redox proteins and enzymes can vary somewhat and lie between 1-40 s^{-1} when cyclic voltammetry measurements are made in phosphate buffer solution on CNT meshes. We should note however that molecular oxygen, the natural co-substrate of the enzyme glucose oxidase, accepts electrons from native GOx at a rate of around 700 s^{-1} [30]. This may suggest that the rate constants measured using simple Laviron theory may _underestimate_ the facility of redox protein turnover at a nanotube modified electrode. This idea is pursued in the next section where the intrinsically dispersive nature of the adsorbed enzyme system is emphasized. This dispersive spread in kinetic activity is not recognised by the Laviron model, which predicts a linear variation of peak separation with lnv, and a single value for the rate constant. In the next section we suggest that the technique of potential step chronoamperometry provides a convenient method to both identify, and monitor the extent of, kinetic dispersion in a surface adsorbed redox system and we examine the response of the GOx immobilized on SWCNT /Nafion modified glassy carbon and gold electrodes.

Determination of flavin group redox kinetics via Potential Step Chronoamperometry: the effect of kinetic dispersion

Cyclic voltammetry does not always provide the optimum route to kinetic parameters. It can be difficult to distinguish between Ohmic drop and kinetic effects when investigating the variation of the voltammetric response with sweep rate. Potential step techniques may be used to calculate electron transfer rate constants for redox systems immobilised on electrodes.

For both gold and glassy carbon, the potential was stepped from a value just before the cathodic peak to a value just after the anodic peak and back again. Hence the potential was stepped from -0.5 to -0.3 V to investigate oxidation, and then from -0.3 to -0.5 V to analyse the reduction process. Figure 18 shows a typical outcome of such an experiment.
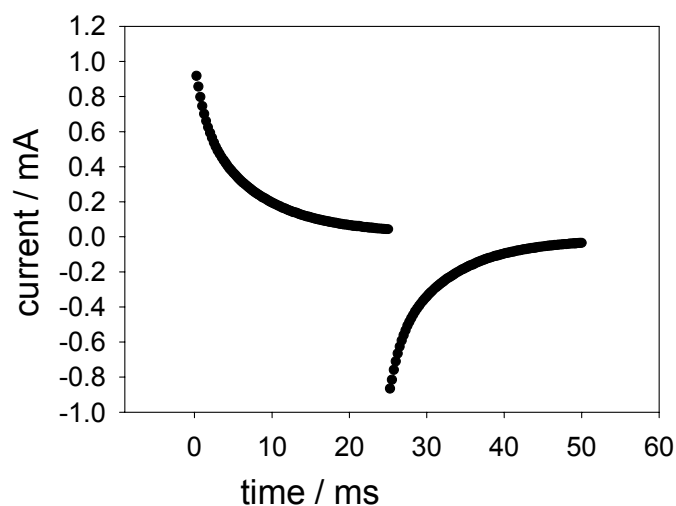
Figure 18. Typical outcome of a potential step experiment across the FAD oxidation and reduction potentials for a SWCNT/GOx/Nafion-modified gold electrode. The electrolyte used was a 50 mM phosphate buffer (pH 7).

The analysis of the current versus time response to a potential step of arbitary magnitude has been recently described by Lyons [30]. We review this material for convenience here. We initially consider the transient current response obtained to a large amplitude potential step perturbation applied to a surface immobilized redox couple A/B. We let Γ_j (j = A,B) represent the surface coverage (units: mol cm^{-2}) of component j of the redox couple, and define the total surface coverage as $\Gamma_\Sigma = \Gamma_A + \Gamma_B$. We initially assume that the surface redox reaction is irreversible with a rate equation given by:

$$-\frac{d\Gamma_A}{dt} = \frac{d\Gamma_B}{dt} = k_{ET}\Gamma_A \tag{23}$$

where the heterogeneous electrochemical rate constant (units: s^{-1}) is of the Butler-Volmer type and is given by

$$k_{ET} = k_{ET}{}^0 \exp[\beta\xi] \tag{24}$$

where k^0 denotes the standard rate constant, β is the symmetry factor and ξ denotes a normalized potential given by $\xi = \frac{F}{RT}\left(E - E^0_{A/B}\right)$. The current response to the applied potential step is given by

$$i(t) = nFAf_\Sigma(t) = nFAk_{ET}\Gamma_A(t) \tag{25}$$

where f_Σ denotes the net flux (units: mol cm^{-2} s^{-1}), n denotes the number of electrons transferred in the surface redox process, A denotes the geometric area of the electrode and F is the Faraday constant.

The variation of surface coverage with time is obtained via integration of eqn.1 subject to the initial condition that at $t = 0$ $\Gamma_A = \Gamma_\Sigma$. Hence integration of eqn.23 immediately yields that

$$\Gamma_A(t) = \Gamma_\Sigma \exp[-k_{ET}t] \tag{26}$$

and the surface redox transition obeys first order kinetics. Hence the current response is expected to follow a simple exponential decay   and is given by

$$i(t) = k_{ET}Q\exp[-k_{ET}t] \tag{27}$$

where the charge Q is related to the surface coverage of electroactive groups via the expression $Q = nFA\Gamma_\Sigma$. This expression has been used by Finklea [31], Chidsey [32] , Miller and co-workers [33] and by Forster and Faulkner [34] to examine the dynamics of self assembled monolayer systems. Hence we conclude that the variation of current with time for a simple surface redox transformation is described by simple first-order kinetics. This means that, ideally, a plot of natural logarithm of the current against time should be linear, with a slope giving directly the heterogeneous electrochemical rate constant k_{ET}.

We can readily extend the analysis to consider a quasi-reversible surface reaction. In this case the rate equation for the surface redox reaction is given by

$$-\frac{d\Gamma_A}{dt} = k_{ET}\Gamma_A - k'_{ET}\Gamma_B \tag{28}$$

where the heterogeneous rate constant for the reverse step is given by $k'_{ET} = k_{ET}{}^0\exp[-(1-\beta)\xi]$. We can integrate eqn.28 using the initial condition $t = 0$ $\Gamma_A = \Gamma_\Sigma$ $\Gamma_B = 0$ to obtain

$$\Gamma_A(t) = \Gamma_\Sigma\left\{\frac{1+(k_{ET}/k'_{ET})\exp[-k_\Sigma t]}{1+(k_{ET}/k'_{ET})}\right\} \tag{29}$$

where we note that $k_\Sigma = k_{ET} + k'_{ET}$. At any time t we also note that $\Gamma_A(t) + \Gamma_B(t) = \Gamma_\Sigma$ and so we also obtain that

$$\Gamma_B(t) = \Gamma_\Sigma\left\{\frac{(k_{ET}/k'_{ET})(1-\exp[-k_\Sigma t])}{1+(k_{ET}/k'_{ET})}\right\} \tag{30}$$

The net current response is therefore given by

$$i(t) = nFA\{k_{ET}\Gamma_A(t) + k'_{ET}\Gamma_B(t)\} \tag{31}$$

From eqn.29, eqn.30 and eqn.31 we immediately obtain

$$i(t) = nFAk_\Sigma\Gamma_\Sigma\exp[-k_\Sigma t] = i_0\exp[-k_\Sigma t] \tag{32}$$

Again a simple exponential decay in current with time is predicted. A plot of ln i versus t is linear with intercept given by $nFAk_\Sigma\Gamma_\Sigma$ and a slope given by $-k_\Sigma$. Hence the surface redox kinetics can be completely resolved using the potential step technique.

Figure 19 shows a plot of the logarithm of the normalised current against time obtained for the oxidation of FADH2 and the reduction of FAD at a SWCNT/GOx/Nafion-modified gold electrode. The current at zero time (i0) is simply estimated using Figure 18. It can be seen that the chronoamperometric transients displayed in Figure 19 are not linear. Consequently the prediction of a simple first order kinetic situation is not maintained experimentally, and the modellistic analysis must be adjusted accordingly. It is also clear that the deviation of the semilogarithmic plot from simple linear first order kinetic behaviour presents in a very direct way the fact that the surface redox kinetics are more complex than expected . This is a compelling reason why the technique of potential step chronoamperometry is to be preferred over that of cyclic voltammetry.

This discrepancy is attributed to the energetic non- equivalence of the GOx molecules on the nanotubes. It is safe to assume that the orientation of the protein structure with respect to the nanotube

platform is not uniform. This means that the FAD sites in each molecule are various distances from the nanotubes, so a variation in the magnitude of the rate constant quantifying the ET kinetics between the flavin active site and the nanotube surface is observed. There exists an undefined spatial relationship between the protein and the SWCNTs. Furthermore, some sites on the nanotubes are more active than others due to the presence or absence of oxygenated defects. Also, it has been established that SWCNTs show a range of conductivity [1]. These factors all serve to increase the spread of observed rate constants.

(a)

(b)
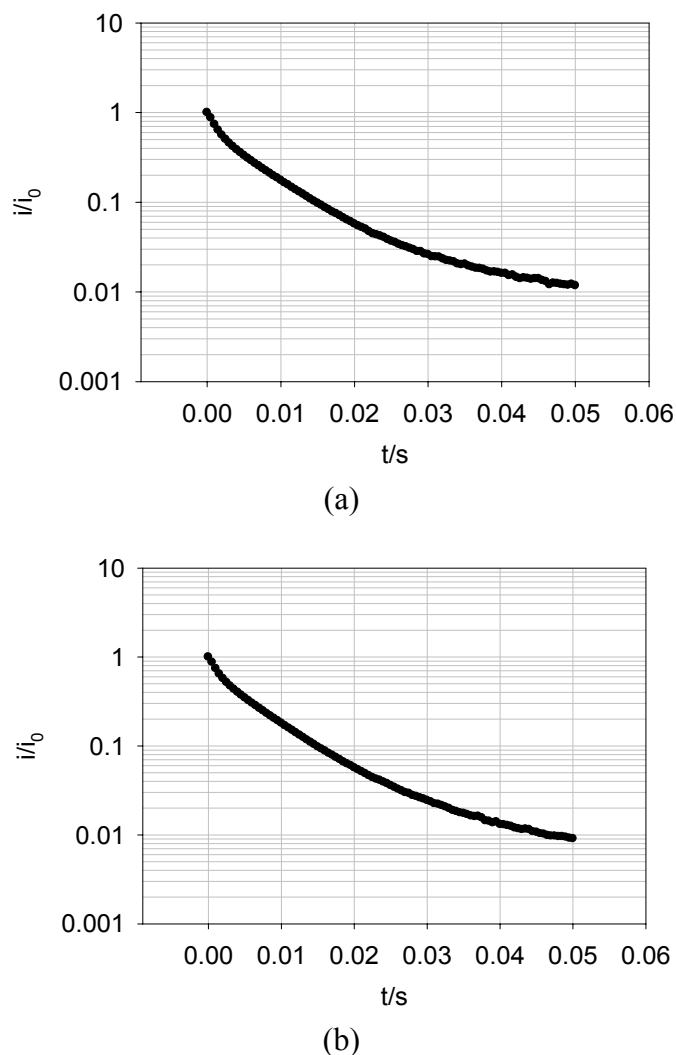
Figure 19. Semi – logarithmic chronoamperometric plot recorded for (a) the oxidation of $FADH_2$ and (b) the reduction of FAD at a SWCNT/GOx/Nafion-modified gold electrode. The electrolyte used was a 50 mM phosphate buffer (pH 7).

The Bi-exponential Model

In situations such as these, in which there is a serious deviation from first-order kinetics, current transients and kinetic plots are sometimes examined on the basis of the bi-exponential model. The

physical interpretation of this model is that every active enzyme site in the system is in one of two distinct environments, characterised by the 'fast' and 'slow' rate constants k_f and k_s. Examples of this approach can be found in the literature [35, 36] . In the bi-exponential model the simple single exponential decay is replaced by a two term expression of the following type

$$\frac{i}{i_0} = A\exp(-k_f t) + B\exp(-k_s t) \tag{33}$$

where A and B are coefficients representing the relative weights associated with the processes having the 'fast' and 'slow' rate constants k_f and k_s, respectively. Hence one fits the experimental current transients to eqn.33 and from the NLLS analysis one extracts values for the four parameters k_f, k_s, A and B. The results of the NLLS fitting (using SIGMAPLOT version 9, www.systat.com) of the four parameter biexponential model to the chronoamperometric transient data are presented in figure 20. The data obtained in our potential step measurements fit nicely to this model (correlation coefficient ~ 0.999) and the calculated rate constants (with standard deviations) are shown in Table 1.

Table 1. Four parameter NLLS Biexponential fitting of potential step chronoamperometry transients for GOx/SWCNT/Nafion modified Au and GC electrodes.

ELECTRODE	k_f / s^{-1}	k_s / s^{-1}	A/B
Au OXIDATION	583 ± 21	11 ± 2	0.8
Au REDUCTION	541 ± 19	103 ± 2	1.1
GC OXIDATION	897 ± 18	197 ± 4	2.1
GC REDUCTION	702 ± 13	115 ± 5	4.9

The ratio A/B is an indication of the extent to which each environment contributes to the observed current. A large value suggests that the 'fast' environment dominates. The rate constants are of the same order of magnitude as those shown by the turnover of native glucose oxidase by molecular oxygen . However the assumption on which the biexponential model is based is rather crude. It seems reasonable to assume that the number of distinct environments experienced by the adsorbed enzyme must be considerably larger than two. Of course, the biexponential expression may be extended to incorporate any number of environments resulting in a multiexponential expression, but when this is done, calculated rate constants quickly become unreliable, with very large standard deviations. This is because of the large number of parameters required for fitting.

The Gaussian Model

Typically when heterogeneous systems such as hydrated oxide thin films, fluorescence decay in membranes, semiconductor nanoparticle dispersions are subjected to a kinetic analysis, curved

semilogarithmic plots are often observed (as presented in figure 19) when the data is tested for first order kinetics. Albery and co-workers [37] have proposed that it is possible to present an alternative model for kinetics in these dispersed systems. In this approach one assumes a Gaussian distribution in the <u>free energy of activation</u> for the kinetic process and consequently in the <u>logarithm</u> of the rate constant about some mean value. In short a log-normal distribution is assumed [38]. Hence one single adjustable parameter is only introduced- the width γ of the distribution. When $\gamma = 0$ there is no dispersion and the system behaves in a classical homogeneous fashion and first order kinetics are observed.
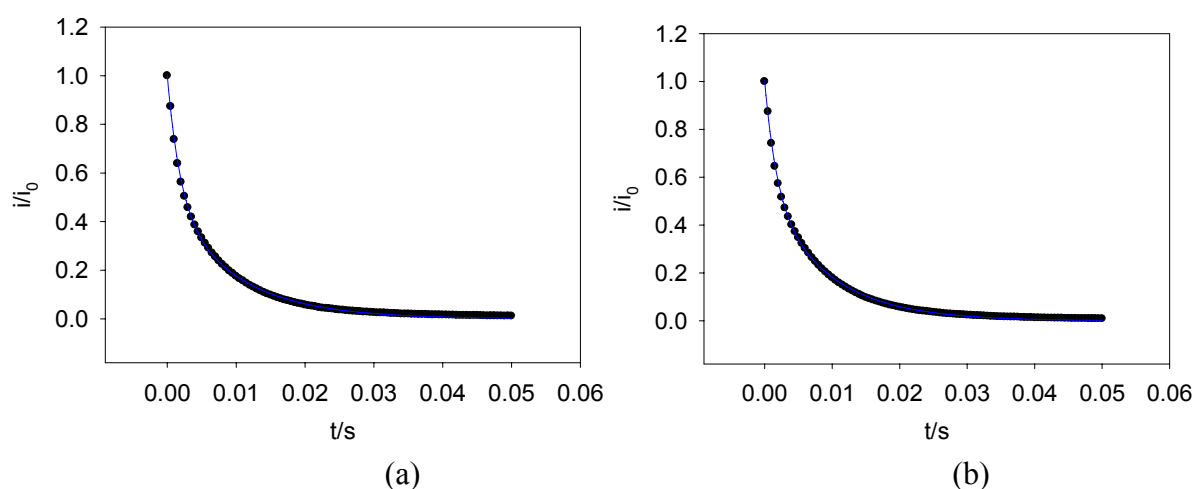
Figure 20. Potential step chronoamperometry transients recorded for (a) GOx oxidation (potential step -500 to - 300 mV) and (b) GOx reduction (potential step from – 300 to – 500 mV) fit via SIGMAPLOT to the four parameter biexponential model. Phosphate buffer solution pH 7.

We assume that the free energy of activation for the enzyme redox process is given by the following expression

$$\Delta G^* = \langle \Delta G^* \rangle - RT\gamma \chi \qquad (34)$$

where $\langle \Delta G^* \rangle$ denotes the mean free energy of activation and γ denotes the spread parameter. The quantity χ denotes the co-ordinate characterizing the Gaussian Distribution. Note that when $\gamma = 0$ $\Delta G^* = \langle \Delta G^* \rangle$ and there is no dispersive spread. The kinetics are simple first order. We define $\langle k_{ET} \rangle$ to be the heterogeneous electron transfer rate constant for the most probable state and write that the dispersion in first order rate constants is

$$k_{ET} = \langle k_{ET} \rangle \exp[\gamma \chi] \qquad (35)$$

We also define a normalized time τ related to the mean rate constant $\langle k_{ET} \rangle$ via $\tau = \langle k_{ET} \rangle t$. Now the first order rate equation for surface adsorbed enzyme is given by

$$-\frac{d\Gamma}{dt} = k_{ET}\Gamma = \langle k_{ET} \rangle \exp[\gamma \chi]\Gamma \qquad (36)$$

Integrating we obtain

$$\int_{\Gamma_{x,0}}^{\Gamma_{x,t}} \frac{d\Gamma}{\Gamma} = -\langle k_{ET} \rangle \exp[\gamma \chi] \int_0^t dt \tag{37}$$

and so simplifying we obtain

$$\frac{\Gamma_\chi(\tau)}{\Gamma_{\chi,0}} = \exp\left[-\tau \exp[\gamma \chi]\right] \tag{38}$$

We now integrate across the Gaussian distribution and note that the decay of the surface concentration of species Γ from their initial value Γ_0 is given by

$$\frac{\Gamma}{\Gamma_0} = \frac{\int_{-\infty}^{\infty} \exp\left[-\chi^2\right].\exp\left[-\tau \exp[\gamma\chi]\right] d\chi}{\int_{-\infty}^{\infty} \exp\left[-\chi^2\right] d\chi} = \frac{1}{\sqrt{\pi}} \int_{-\infty}^{\infty} \exp\left[-\chi^2\right].\exp\left[-\tau \exp[\gamma\chi]\right] d\chi \tag{39}$$

where we note that the Gaussian integral takes the following form

$$\int_{-\infty}^{\infty} \exp\left[-\chi^2\right] d\chi = \sqrt{\pi} \tag{40}$$

It is satisfactory to note that when $\gamma = 0$ corresponding to the absence of kinetic dispersion, eqn. 39 reduces to

$$\frac{\Gamma}{\Gamma_0} = \exp[-\tau] \tag{41}$$

corresponding to simple first order exponential decay.

Now the net current i is given by

$$
\begin{aligned}
i &= nFAf_\Sigma = nFAk_{ET}\Gamma = nFA\langle k_{ET}\rangle\Gamma \\
&= nFA\langle k_{ET}\rangle\Gamma_0 \pi^{-1/2} \int_{-\infty}^{\infty} \exp[\gamma\chi]\exp\left[-\chi^2\right]\exp\left[-\tau \exp[\gamma\chi]\right] d\chi \\
&= nFA\langle k_{ET}\rangle\Gamma_0 \pi^{-1/2} I(\gamma, \chi, \tau)
\end{aligned}
\tag{42}
$$

The integral $I(\gamma, \chi, \tau)$ on the rhs of eqn.42 must be solved numerically. We note that:

$$I(\gamma, \chi, \tau) = I_1(\gamma, \chi, \tau) + I_2(\gamma, \chi, \tau) \tag{43}$$

where

$$I_1(\gamma, \chi, \tau) = \int_{-\infty}^{0} \exp[\gamma\chi]\exp\left[-\chi^2\right]\exp\left[-\tau \exp[\gamma\chi]\right] d\chi$$

$$I_2(\gamma, \chi, \tau) = \int_{0}^{\infty} \exp[\gamma\chi]\exp\left[-\chi^2\right]\exp\left[-\tau \exp[\gamma\chi]\right] d\chi \tag{44}$$

To proceed further we follow the procedure first outlined by Albery and co-workers [37] and utilize the following transformation:

$$
\begin{aligned}
\chi < 0 \quad \chi = \ln\lambda \quad d\chi = \lambda^{-1} d\lambda \\
\chi > 0 \quad \chi = -\ln\lambda \quad d\chi = -\lambda^{-1} d\lambda
\end{aligned}
\tag{45}
$$

Hence when

$$\chi = \pm\infty \quad \lambda = 0$$
$$\chi = 0 \quad \lambda = 1$$

(46)

and so the integrals outlined in eqn.44 reduce to

$$I_1 = \int_0^1 \exp[\gamma \ln \lambda] \exp\left[-(\ln \lambda)^2\right] \exp\left[-\tau \exp[\gamma \ln \lambda]\right] \lambda^{-1} d\lambda$$

$$= \int_0^1 \lambda^\gamma \exp\left[-(\ln \lambda)^2\right] \exp\left[-\tau\lambda^\gamma\right] \lambda^{-1} d\lambda$$

(47)

$$I_2 = \int_0^1 \exp[-\gamma \ln \lambda] \exp\left[-(\ln \lambda)^2\right] \exp\left[-\tau \exp[-\gamma \ln \lambda]\right] \lambda^{-1} d\lambda$$

$$= \int_0^1 \lambda^{-\gamma} \exp\left[-(\ln \lambda)^2\right] \exp\left[-\tau\lambda^{-\gamma}\right] \lambda^{-1} d\lambda$$

where we have used the following identities

$$\exp[\gamma \ln \lambda] = \exp[\ln \lambda]^\gamma = \lambda^\gamma$$
$$\exp[-\gamma \ln \lambda] = \exp[\ln \lambda]^{-\gamma} = \lambda^{-\gamma}$$

(48)

Hence we obtain that

$$I(\gamma, \chi, \tau) = \int_0^1 G(\lambda) d\lambda$$

(49)

where we define

$$G(\lambda) = \lambda^{-1} \exp\left[-(\ln \lambda)^2\right] \left\{ \lambda^\gamma \exp\left[-\lambda^\gamma \tau\right] + \lambda^{-\gamma} \exp\left[-\lambda^{-\gamma}\tau\right] \right\}$$

(50)

Hence the current transient may be computed from eqn.42 using eqn.49 and eqn.50. Similarly, the integral outlined in eqn.39 may be integrated in a similar manner

$$\frac{\Gamma}{\Gamma_0} = \frac{1}{\sqrt{\pi}} \int_{-\infty}^{\infty} \exp\left[-\chi^2\right].\exp\left[-\tau \exp[\gamma\chi]\right] d\chi$$

$$= \frac{1}{\sqrt{\pi}} \int_0^1 F(\lambda) d\lambda$$

(51)

where

$$F(\lambda) = \lambda^{-1} \exp\left[-(\ln \lambda)^2\right] \left\{ \exp\left[-\lambda^\gamma \tau\right] + \exp\left[-\lambda^{-\gamma}\tau\right] \right\}$$

(52)

The population of Gaussian distributed redox states computed numerically via the extended Simpsons rule [37] with $\gamma = 2$ is outlined in figure 21.
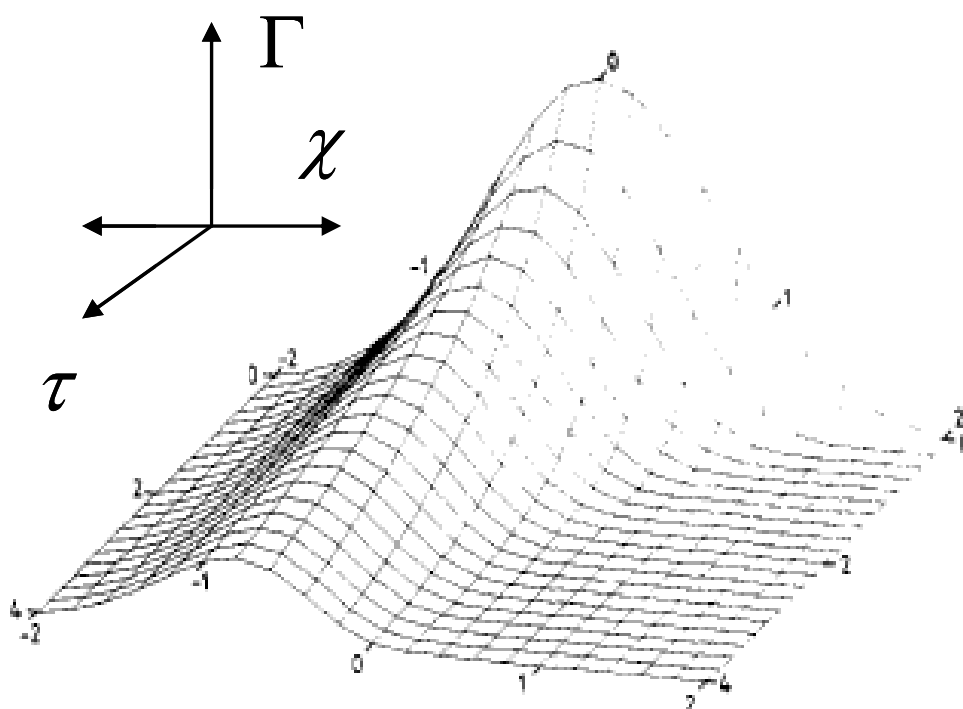
Figure 21. The decay of the Gaussian population calculated using eqn.51 with spread parameter $\gamma = 2$.

We note from this 3D surface plot calculated from eqn.51 that as the reaction proceeds (as τ increases) the original symmetrical Gaussian profile becomes skewed to those species with lower rate constants. These slower species predominate in the latter stages of a chronoamperometric experiment giving rise to the type of curvature seen in the semi-logarithmic plots presented in figure 20. It also indicates why a simple bi-exponential model is not the best method for analysis of chronoamperometric transients. The values for the fast and slow rate constants extracted from the latter type of analysis will depend on the magnitude of the time window over which the potential pulse is applied. Hence the Gaussian model with the derivation of an average rate constant along with a measure of the dispersive spread γ is a much better approach. It should be noted that when analyzing current transients the faster redox sites make a greater contribution to the observed redox current.

Typical theoretical current transients computed via eqn.42 using eqn.49 and eqn.50 are presented below in figure 22. We note that the current decays more rapidly as the value of the Gaussian spread parameter γ increases. We also note that the deviation from linearity in the semi logarithmic plot presented in figure 22b also increases significantly when the dispersive spread parameter γ increases.

The calculations derived using eqn.51 are also presented in terms of a double logarithmic plot in figure 23. The latter form a working curve of $\ln\left(\Gamma/\Gamma_0\right)$ versus $\ln\tau$. Experimentally derived data may be readily recast into equivalent format and the experimental curve can then be matched to the theoretical curve by adjusting the displacements on both the x and y axes. In this way the Gaussian spread parameter may be determined.

Alternatively, to determine a value of the spread parameter from experimental data one can follow the procedure originally suggested by Albery and co-workers [37]. In this work it was suggested that

the ratio of $\tau_{7/8}$ to $\tau_{1/2}$ be measured where $\tau_{1/2}$ defined the half life of the reaction and $\tau_{7/8}$ defines the time when one eight of the original reactant species remains. The following empirical relationship between γ and the latter parameters has been proposed:

$$\gamma = 0.92 \times \left(\frac{\tau_{7/8}}{\tau_{1/2}} - 3 \right)^{1/2} \tag{53}$$

It was also suggested that the mean rate constant could be evaluated from the latter relationship

$$\langle k_{ET} \rangle = \frac{1}{\tau_{1/e}} \tag{54}$$

where $\tau_{1/e}$ is the time when the current has decayed to $1/e$ (~0.37) of its initial value. In practical terms, this is simply the time when the ratio i / i_0 is approximately 0.63, or ln (i /i_0) is around -0.46. Our experimental findings, measured at pH 7 are summarized in Table 2. It is clear from this data that the rate constant as estimated from the simple Laviron analysis is considerably less than that estimated using the Gaussian model. Hence we conclude that the neglect of kinetic dispersion will result in a serious under-estimation of the heterogeneous electrochemical rate constant for the redox transformation of an immobilized redox active moiety.
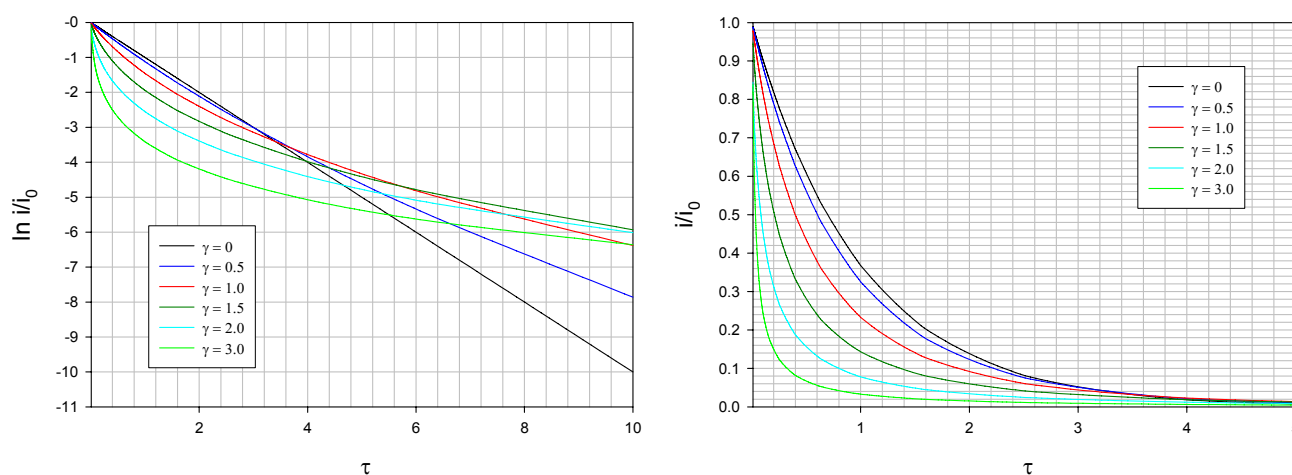
Figure 22. (a) Typical normalized current transients calculated for various values of the Gaussian spread parameter γ. (b) Semi-logarithmic representation of the data presented in fig.22(a), again as a function of spread parameter.

It is well established that the redox chemistry of the FAD/FADH$_2$ reaction is pH dependent. We therefore measured the heterogeneous electron transfer rate constant for the latter process as a function of solution pH via analysis of the potential step chronoamperometric response and using the Gaussian dispersive spread model. Our findings are presented in table 3. Over the pH range studied, it is clear that the rate of the redox transition increases with increasing pH, whereas the latter does not influence the degree of kinetic dispersion to any appreciable extent. The values determined for the rate constants are quite large and imply an efficient turnover of the redox enzyme oxidation state at the carbon nanotube surface. This observation augers well for biosensor applications.
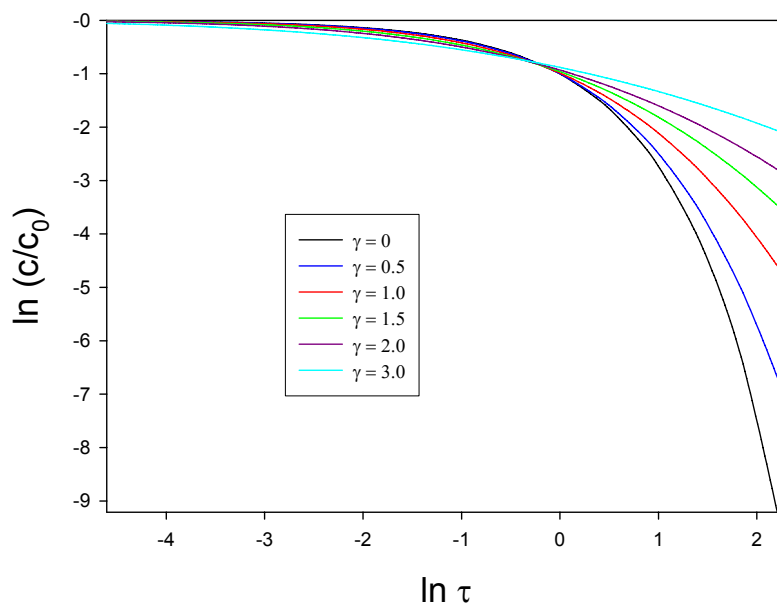
Figure 23. Typical double logarithmic plots calculated for various values of the Gaussian spread parameter γ.

Table 2. Analysis of chronoamperometric transients via
the simple Laviron model and via the Gaussian spread model.

Working Electrode	Laviron model k_{ET} / s^{-1}	Gaussian model $<k_{ET}>$ / s^{-1}	Spread Parameter γ
Au/SWCNT/GOx/Nafion	19	830	0.9
GC/SWCNT/GOx/Nafion	18	950	1.2

Table 3. Analysis of the FAD/FADH$_2$ ET kinetics as function of solution pH.

Solution pH	mean rate constant $<k_{ET}>$ / s^{-1}	Gaussian spread parameter γ
5.2	500	0.8
5.9	625	0.8
7.0	830	0.9
8.0	1250	1.0
8.9	1600	1.0

Conclusions

In this paper we have reported in detail on the redox behaviour of SWCNTs randomly dispersed on gold and glassy carbon electrode surfaces. We have demonstrated that examining the electrochemical response of simple solution phase redox couples may be used to indirectly probe the properties of the immobilized nanotube meshes. We have used a simple technique to adsorb glucose oxidase onto SWCNT-modified gold and glassy carbon electrodes and shown that well defined voltammetric responses can be obtained at these enzyme modified nanotube meshes and the kinetics of the $FAD/FADH_2$ redox transformation may be directly quantified. We have also demonstrated that adsorbed enzymes exhibit significant kinetic dispersion, and that the dispersion is best subjected to analysis via potential step chronoamperometry. This conclusion is in contrast to current practice where linear potential sweep voltammetry is often the technique adopted for the quantitative analysis of kinetic data of surface immobilized redox species. In our quantitative analysis we have utilised a sophisticated analysis developed some years ago by Albery [37], which assumes that curved, semi-logarithmic kinetic plots can be fitted using a Gaussian kinetic model. The extension of the Gaussian kinetic model to linear potential sweep voltammetry is currently underway and will be reported in a subsequent paper.

The results presented clearly show that rate constants calculated using potential step chronoamperometry are significantly higher than those found via voltammetry and using the well established Laviron analysis which neglects kinetic dispersion effects. The flavin redox chemistry has been probed as a function of support electrode and solution pH. We note that the methods and theoretical analysis presented here can easily be extended to immobilize, and clarify the direct electrochemistry of, other enzymes and redox proteins.

Acknowledgements

References and Notes

1. Iijima, S. Helical Microtubules of Graphitic Carbon. *Nature* **1991**, *354*, 56-58.
2. (a) Goodring, J.J. Nanostructuring electrodes with carbon nanotubes : A review on electrochemistry   and applications for sensing. *Electrochim. Acta* **2005**, *50*, 3049-3060. (b) Wang, J. Carbon nanotube based electrochemical biosensors: a review. *Electroanalysis* **2005**, *17*, 7-14.
3. Katz, E.; Willner, I. Biomolecule – functionalized carbon nanotubes: applications in nanobioelectronics. *ChemPhysChem* **2004**, *5*, 1084-1104.
4. Kuznetsov, A.M.; Ulstrup, J. Electron transfer in chemistry and biology. **1998**, Wiley, New York.
5. Habermuller, K.; Mosbach, M.; Schuhmann, W. Electron transfer mechanisms in amperometric biosensors. *Fresenius J. Anal. Chem.* **2000**, *366*, 560-568.

6. Schuhmann, W. Amperometric enzyme biosensors based on optimized electron transfer pathways and non-manual immobilization procedures. *Rev. Mol. Biotechnol.* **2002**, *82*, 425-441.

7. Guiseppi-Elie, A.; Lei, C.; Baughman, R. H. Direct Electron Transfer of Glucose Oxidase of Carbon Nanotubes. *Nanotechnology* **2002**, *13*, 559-564.

8. Wang, J.X.; Musameh, M.; Lin, Y. Solubilization of carbon nanotubes by Nafion toward the preparation of amperometric biosensors. *J. Am. Chem. Soc.* **2003**, *125*, 2408-2409.

9. Wang, J. ; Musameh, M. Carbon nanotube/Teflon composite electrochemical sensors and biosensors. *Anal. Chem.* **2003**, *75*, 2075-2079.

10. Wang, G.; Xu, J.J.; Chen, H.Y. Interfacing cytochrome c to electrodes with a DNA-carbon nanotube composite film. *Electrochem. Commun.* **2002**, *4*, 506-509.

11. Yamamoto, K.; Shi, G.; Zhou, T.; Xu, F.; Xu, J.; Kato, T.; Jin, J.J.; Jin, L. Study of carbon nanotubes-HRP modified electrode and its application for novel on line biosensors. *Analyst* **2003**, *128*, 249- 254.

12. (a) Goodring, J.J.; Wibowo, R.; Liu, J.; Yang, W.; Losic, D.; Orbons, S.; Mearns, F.J.; Shapter, J.G.; Hibbert, D.B. Protein electrochemistry using aligned carbon nanotube arrays. *J. Am. Chem. Soc*. **2003**, *125*, 9006-9007. (b) Liu, J.; Chou, A.; Rahmat, W.; Paddon-Row, M.N.; Goodring, J.J. Achieving direct electrical connection to glucose oxidase using aligned single walled carbon nanotube arrays. *Electroanalysis* **2005**, *17*, 38-46.

13. Albery, W. J.; Bartlett, P. N.; Wilde, C. P.; Darwent, J. R. A General Model for Dispersed Kinetics in Heterogeneous Systems. *J. Am. Chem. Soc.* **1985**, *107*, 1854-1858.

14. Nicholson, R. S. Theory and Application of Cyclic Voltammetry for Measurement of Electrode Reaction Kinetics. *Anal. Chem.* **1965**, *37,* 1351-1355.

15. Nugent, J.M.; Santhanam, K.S.V.; Rubio, A.; Ajayan, P.M. Fast electron transfer kinetics on multiwalled carbon nanotube microbundle electrodes. *Nano Lett.* **2001**, *1*, 87-91.

16. Cai, C.; Chen, J. Direct Electron Transfer of Glucose Oxidase promoted by Carbon Nanotubes. *Anal. Biochem.* **2004**, *332*, 75-83.

17. Diao, P.; Liu, Z. Electrochemistry at chemically assembled single wall carbon nanotube arrays. *J. Phys. Chem. B.* **2005**, *109*, 20906-20913.

18. Bard, A.J.; Faulkner, L.R. *Electrochemical Methods*, Wiley, New York, **2001**. Chapter 10, pp.368-416.

19. Laviron, E. General Expression for the Linear Potential Sweep Voltammogram in the case of Diffusionless Electrochemical Systems. *J. Electroanal. Chem.* **1979**, *101*, 19-28.

20. Wang, J., Musameh, M., Lin, Y. Solubilization of carbon nanotubes by Nafion toward the preparation of amperometric biosensors. *J.Am, Chem. Soc.*, **2003**, 125, 2408-2409.

21. O'Connell, M.J.; Boul, P.; Ericson, L.M.; Huffman, C.; Wang, Y.; Haroz, E.; Kuper, C.; Tour, J.; Ausman, K.D.; Smalley, R.E. Reversible water-solubilization of single walled carbon nanotubes by polymer wrapping. *Chem. Phys. Lett.* **2001**, *342*, 265-271.

22. (a) Smith, C.P.; White, H.S. Theory of the interfacial potential distribution and reversible voltammetric response of electrodes coated with electroactive molecular films. *Anal. Chem.* **1992**, *64*, 2398-2405. (b) Ohtani, M.; Kuwabata, S.; Yoneyama, H. Voltammetric response accompanied by inclusion of ion pairs and triple ion formation of electrodes coated with an electroactive monolayer film. *Anal. Chem.* **1997**, *69*, 1045-1053.

23. (a) Brown, A.P.; Anson, F.C. Cyclic and differential pulse voltammetric behaviour of reactants confined to electrode surface. *Anal. Chem.* **1977**, *49*, 1589-1595. (b) Honeychurch, M.J.; Rechnitz, G.A. Voltammetry of adsorbed molecules. Part 1. Reversible Redox systems. *Electroanalysis,* **1998**, *10*, 285-293. (c) Honeychurch, M.J.; Rechnitz, G.A. Voltammetry of adsorbed molecules. Part 2. Irreversible redox systems. *Electroanalysis* **1998**, *10*, 453-457.

24 Shiryava, I.M.; Collman, J.P.; Boulatov, R.; Sunderland, C.J. Non ideal electrochemical behaviour of biomimetic iron porphyrins: interfacial potential distribution across multilayer films. *Anal. Chem.* **2003**, *75*, 494-502.

25. Li, J.; Cassell, A.; Delzeit, L.; Han, J.; Meyyappan, M. Novel three dimensional electrodes: electrochemical properties of carbon nanotune assemblies. *J. Phys. Chem. B* **2002**, *106*, 9299-9305.

26. Roullier, L.; Laviron, E. Effect of uncompensated ohmic drop in surface linear potential sweep voltammetry. Application to the determination of surface rate constants. *J. Electroanal. Chem.* **1983**, *157*, 193-203.

27. Liang, W.; Zhuobin, Y. Direct Electrochemistry of Glucose Oxidase at a Gold Electrode Modified with Single-Wall Carbon Nanotubes. *Sensors* **2003**, *3*, 544-554.

28. Yin, Y.; Lu, Y.; Wu, P.; Cai, C. Direct electrochemistry of redox proteins and enzymes promoted by carbon nanotubes. *Sensors* **2005**, *5*, 220-234.

29. Wang, M.; Shen, Y.; Liu, Y.; Wang, T.; Zhao, F.; Liu, B.; Dong, S. Direct electrochemistry of microperoxidase 11 using carbon nanotube modified electrodes. *J. Electroanal. Chem.* **2005**, *578*, 121-127.

30. Lyons, M.E.G. Mediated electron transfer at redox active monolayers. Part 2. Analysis of the chronoamperometric response to a potential step perturbation. *Sensors* **2002**, *2*, 314-330.

31. (a) Finklea, H.O.; Liu, L.; Ravenscroft, M.S.; Punturi, S. Multiple electron tunneling paths across self-assembled monolayers of alkanethiols with attached ruthenium(II/III) redox centers. *J. Phys. Chem.* **1996**, *100*, 18852-18858. (b) Finklea, H.O. Consequences of a potential dependent transfer coefficient in ac voltammetry and in coupled electron-proton transfer for attached redox couples. *J. Electroanal. Chem.* **2001**, *495*, 79-86. (c) Finklea, H.O.; Yoon, K.; Chamberlain, E.; Allen, J.; Haddox, R. Effect of the metal on electron transfer across self-assembled monolayers. *J. Phys. Chem. B* **2001**, *105*, 3088-3092.

32. (a) Chidsey, C.E.D.; Free energy and temperature dependence of electron transfer at the metal-electrolyte interface. *Science* **1991**, *251*, 919-922 .(b) Chidsey, C.E.D.; Bertozzi, C.R.; Putvinski, T.M.; Mujsce, A.M. Coadsorption of ferrocene-terminated and unsubstituted alkanethiols on gold: electroactive self assembled monolayers. *J. Am. Chem. Soc.* **1990**, *112*, 4301-4306.

33. (a) Miller, C.; Cuendet, P.; Gratzel, M. Adsorbed ω- hydroxy thiol monolayers on gold electrodes: evidence for electron tunneling to redox species in solution. *J. Phys. Chem.* **1991**, *95*, 877-886. (b) Miller, C.; Gratzel, M. Electrochemistry at ω-hydroxy thiol coated electrodes.2. Measurement of the density of electronic states distributions for several outer-sphere redox couples. *J. Phys. Chem.* **1991**, *95*, 5225-5233. (c) Becka, A.M.; Miller, C.J. Electrochemistry at ω-hydroxy thiol coated electrodes. 3. Voltage independence of the electron tunneling barrier and measurements of redox kinetics at large overpotentials. *J. Phys. Chem.* **1992**, *96*, 2657-2668.

34. (a) Forster, R.J.; Faulkner, L.R. Electrochemistry of spontaneously adsorbed monolayers. Equilibrium properties and fundamental electron transfer characteristics. *J. Am. Chem. Soc.* **1994**, *116*, 5444-5452. (b) Forster, R.J.; Faulkner, L.R. Electrochemistry of spontaneously adsorbed monolayers. Effects of solvent, potential and temperature on electron transfer dynamics. *J. Am. Chem. Soc.* **1994**, *116*, 5453-5461. (c) Forster, R.J.; O'Kelly, J.P. pH modulated heterogeneous electron transfer across metal/monolayer interfaces. *J. Phys. Chem.* **1996**, *100*, 3695-3704. (d) Forster, R.J.; Keyes, T.E. Tetrazine bridged osmium dimmers: electrochemical vs photoinduced electron transfer. *J. Phys. Chem. B* **2001**, *105*, 8829-8837.

35. Norman, L. L.; Barrett, C. J. Solution Properties of Self-Assembled Amphiphilic Copolymers Determined by Isomerisation Spectroscopy. *J. Phys. Chem. B* **2002**, *106,* 8499-8503.

36. Scott, K.F. Extraction of rate constant distributions from heterogeneous chemical kinetics. *J. Chem. Soc. Faraday I* **1980**, *76*, 2065-2079.

37. Albery, W.J.; Bartlett, P.N.; Wilde, C.P.; Darwent, J.R. A general model for dispersed kinetics in heterogeneous systems. *J. Am. Chem. Soc.* **1985**, *107*, 1854-1858.

38. See for example the excellent Wikipedia definition at http://en.wikipedia.org/wiki/Log-normal_distribution.